Available online at www.sciencedirect.com
SCIENCE DIRECT
Geochimica et Cosmochimica Acta 70 (2006) 3011–3030
Geochimica
www.elsevier.com/locate/gca

Iron isotope fractionation during hydrothermal ore deposition and alteration

Gregor Markl [a,*], Friedhelm von Blanckenburg [b], Thomas Wagner [a]

[a] Institut für Geowissenschaften, Wilhelmstr 56, D-72074 Tübingen, Germany
[b] Institut für Mineralogie, Callinstrasse 3, D-30167 Hannover, Germany

Received 25 July 2005; accepted in revised form 3 February 2006

Abstract

Iron isotopes fractionate during hydrothermal processes. Therefore, the Fe isotope composition of ore-forming minerals characterizes either iron sources or fluid histories. The former potentially serves to distinguish between sedimentary, magmatic or metamorphic iron sources, and the latter allows the reconstruction of precipitation and redox processes. These processes take place during ore formation or alteration. The aim of this contribution is to investigate the suitability of this new isotope method as a probe of ore-related processes. For this purpose 51 samples of iron ores and iron mineral separates from the Schwarzwald region, southwest Germany, were analyzed for their iron isotope composition using multicollector ICP-MS. Further, the ore-forming and ore-altering processes were quantitatively modeled using reaction path calculations. The Schwarzwald mining district hosts mineralizations that formed discontinuously over almost 300 Ma of hydrothermal activity. Primary hematite, siderite and sulfides formed from mixing of meteoric fluids with deeper crustal brines. Later, these minerals were partly dissolved and oxidized, and secondary hematite, goethite and iron arsenates were precipitated. Two types of alteration products formed: (1) primary and high-temperature secondary Fe minerals formed between 120 and 300 °C, and (2) low-temperature secondary Fe minerals formed under supergene conditions (<100 °C). Measured iron isotope compositions are variable and cover a range in δ^{56}Fe between −2.3‰ and +1.3‰. Primary hematite (δ^{56}Fe: −0.5‰ to +0.5‰) precipitated by mixing oxidizing surface waters with a hydrothermal fluid that contained moderately light Fe (δ^{56}Fe: −0.5‰) leached from the crystalline basement. Occasional input of CO_2-rich waters resulted in precipitation of isotopically light siderite (δ^{56}Fe: −1.4 to −0.7‰). The difference between hematite and siderite is compatible with published Fe isotope fractionation factors. The observed range in isotopic compositions can be accounted for by variable fractions of Fe precipitating from the fluid. Therefore, both fluid processes and mass balance can be inferred from Fe isotopes. Supergene weathering of siderite by oxidizing surface waters led to replacement of isotopically light primary siderite by similarly light secondary hematite and goethite, respectively. Because this replacement entails quantitative transfer of iron from precursor mineral to product, no significant isotope fractionation is produced. Hence, Fe isotopes potentially serve to identify precursors in ore alteration products. Goethites from oolitic sedimentary iron ores were also analyzed. Their compositional range appears to indicate oxidative precipitation from relatively uniform Fe dissolved in coastal water. This comprehensive iron isotope study illustrates the potential of the new technique in deciphering ore formation and alteration processes. Isotope ratios are strongly dependent on and highly characteristic of fluid and precipitation histories. Therefore, they are less suitable to provide information on Fe sources. However, it will be possible to unravel the physico-chemical processes leading to the formation, dissolution and redeposition of ores in great detail.

1. Introduction

The stable isotopes of transition metals such as Cr, Fe, Cu, or Mo have recently attracted much attention as possible tools for deciphering geochemical processes (see the review by Johnson et al., 2004a). The observed natural variations of their isotope ratios have been attributed to a number of processes such as fluid–solid reactions (Barling et al., 2001; Rouxel et al., 2003; Albarède, 2004), redox reactions in aqeuous fluids (Matthews et al., 2001; Schauble et al., 2001; Ellis et al., 2002; Welch et al., 2003;

* Corresponding author. Fax: +49 7071 29 3060.
E-mail address: markl@uni-tuebingen.de (G. Markl).

0016-7037/$ - see front matter © 2006 Elsevier Inc. All rights reserved.
doi:10.1016/j.gca.2006.02.028

Anbar et al., 2005), inter-mineral equilibrium fractionation (Polyakov, 1997; Polyakov and Mineev, 2000; Williams et al., 2004), the involvement of micro-organisms (Johnson et al., 2004b), the uptake of metals by marine organisms (Maréchal et al., 2000) or by plants and humans (Walczyk and von Blanckenburg, 2002; Walczyk and von Blanckenburg, 2005). All studies agree that at ambient temperatures both biological and abiotic processes can cause shifts in transition metal isotope ratios of a few permil per mass unit. A demonstration of such fractionations at higher temperatures is still a matter of debate (Zhu et al., 2000, 2002; Beard and Johnson, 2004; Williams et al., 2004). One of the reasons for the absence of clear high-temperature fractionations is that equilibrium isotope fractionation is predicted to decrease with increasing temperature, and the expected shifts are in the range of instrumental detection limits (Polyakov, 1997; Schauble, 2004). Metal isotope fractionation is expected, and has been observed, during hydrothermal ore formation which takes place within an intermediate temperature range and also involves a large range of inorganic aqueous geochemical reactions that would entail isotope fractionation. For Cu isotopes, Zhu et al. (2000) could show that samples of one mineral type from the same deposit exhibits large variations of copper isotope ratios, but it is not clear by which process these variations are caused. Graham et al. (2004) suggested that large shifts in Fe isotope composition (over 4‰ in the $^{56}Fe/^{54}Fe$ ratio) can occur in iron deposits associated with magmatic processes, i.e., in a Cu–Au porphyry–skarn complex. There, the variability was explained by mixtures of iron from different, specifically igneous and sedimentary, sources. The data of Rouxel et al. (2003) indicate that during alteration of oceanic basalts, isotopically light iron is preferentially leached, transported in the fluid and then deposited in hydrothermal Fe–Si deposits, whereas the isotopically heavy iron remains mainly in the basaltic alteration products such as celadonite. This was attributed to a kinetic control during leaching, or to preferential incorporation of the heavier isotope into celadonite. All these early observations suggest that stable transition metal isotopes do indeed have potential as tools in petrogenetic studies, but a conceptual framework for their interpretation is still not in place.

The topic of this contribution is to provide a concept for Fe isotope ratio variations in hydrothermal and supergene iron ores. For this purpose, we report a large new dataset comprising 51 samples of various iron minerals from hydrothermal and sedimentary deposits in a well-investigated ore district of Central Europe, the Schwarzwald in southwest Germany. The purpose of this study is

(1) to investigate the iron isotope variability of primary and secondary iron minerals in a large, geologically diverse ore district formed over a period of 300 million years which has been well described (e.g., Metz et al., 1957; Werner and Franzke, 2001; Werner et al., 2002; Werner and Dennert, 2004; Markl, 2004; Schwinn and Markl, 2005; Schwinn et al., 2006),
(2) to relate the observed isotope fractionation trends to a physico-chemical model of iron ore formation, and
(3) to investigate whether Fe isotopes can be used as predictive tools for ore formation and hydrothermal alteration.

2. Geological context

The Variscan Schwarzwald gneissic and granitic basement and the overlying Triassic Buntsandstein host a large number of hydrothermal vein-type deposits (Fig. 1). Many of them contain various Fe-bearing phases, mainly hematite, goethite and siderite. Within an area of 120 by 40 km, more than 400 individual veins are known. Most of these veins are sub-economic, but they have been mined for Ag, Pb, Zn, Co, U or Cu since Roman times. One deposit (the Clara mine near Wolfach) is still active and exploits a barite–fluorite vein. Based on their mineralogy, several hydrothermal mineralization styles can be distinguished, which are, for example, Sb–Ag-bearing quartz veins (occurring throughout the entire district), Co–Ni–Ag–Bi–U-bearing barite–fluorite veins (in the Wittichen area), Fe–Mn-bearing quartz–barite veins (in the Eisenbach area), Cu–Bi-dominated quartz–barite veins in the area between Freudenstadt and Neubulach in the northern Schwarzwald, or the Pb–Zn–(Ag)-bearing quartz–fluorite assemblages in the Southern Schwarzwald (Metz et al., 1957; Bliedtner and Martin, 1988).

The hydrothermal vein systems are believed to have formed by mixing of ascending deep-seated, relatively reduced formation waters with infiltrating meteoric, oxidizing surface waters (Fig. 2; Werner and Dennert, 2004). Based on C, S, H and O isotope studies, the deep-seated fluid was chemically surprisingly uniform in space and time, had a temperature of around 300–350 °C and leached metals (including the iron) from the basement granites and gneisses of the Schwarzwald in 7–8 km depth (Schwinn and Markl, 2005; Schwinn et al., 2006). The surface waters passed through various sedimentary units of Lower Triassic to Upper Jurassic age; some of these strata contain significant amounts of Fe as hematite, goethite or chlorite (Fig. 2). The mixing of the two fluids occurred at a depth of about 1–2 km and the temperature of vein formation depended on the mixing ratio of the two fluids (Schwinn et al., 2006). At this stage, hematite and/or siderite were precipitated as primary Fe-bearing phases, reflecting the specific fluid compositions involved (primary deposits "pD" on Fig. 2). Support for this model comes from the observation that the crystalline rocks show abundant secondary alteration, with chloritization of biotite and sericitization and albitization of feldspars being the most notable alteration reactions. Oxygen isotope investigations of Simon and Hoefs (1987) and Hoefs and Emmermann (1983) indicate the interaction of a meteoric fluid with the basement rocks at temperatures well below 500 °C.

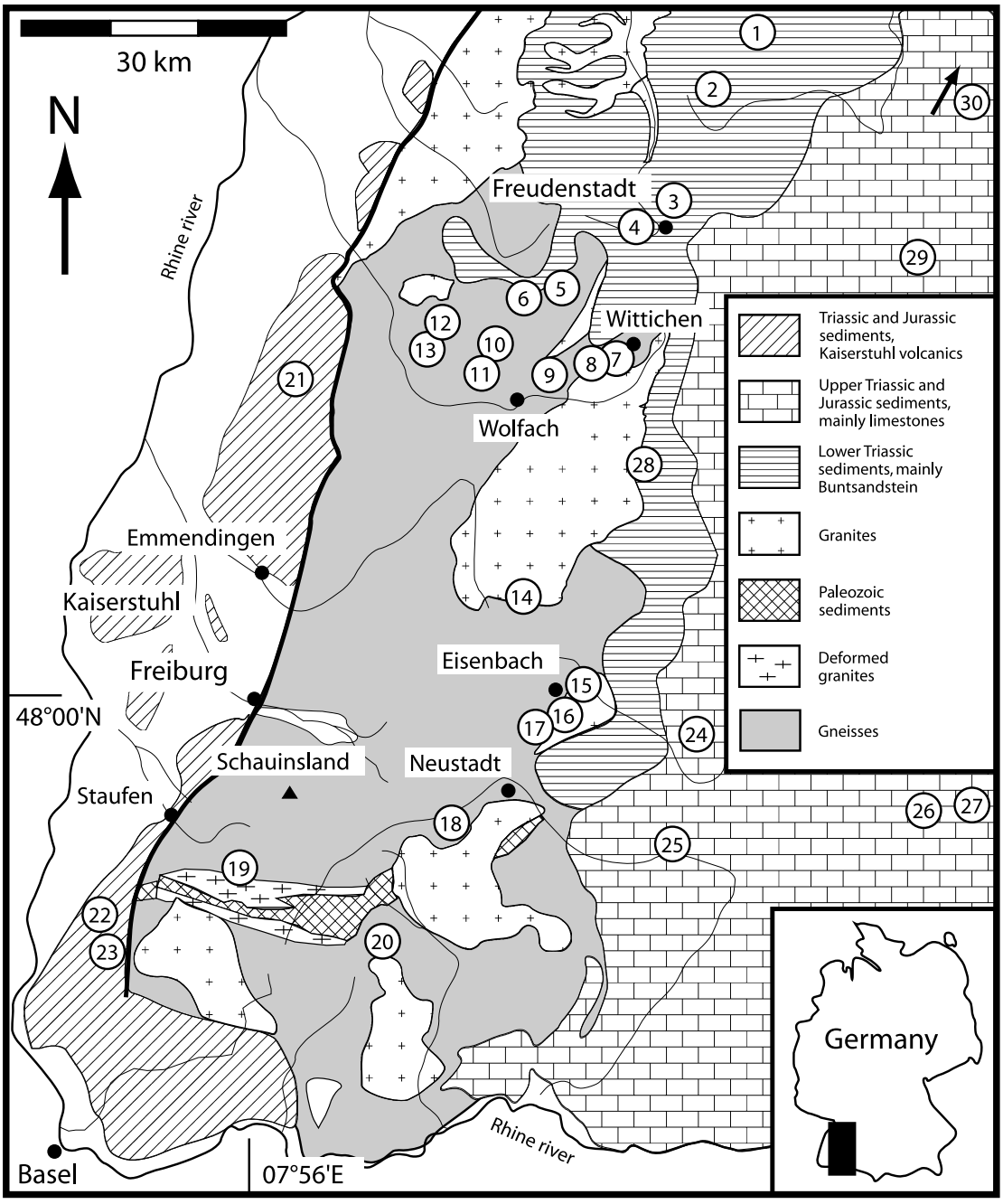

Fig. 1. Simplified geological map of the Schwarzwald region in southwest Germany with sample locations. The numbers refer to Table 1.

Based on observed structures, fluid inclusion studies and a comparison with similar veins in the Rhenish Massif (e.g., Wagner and Cook, 2000; Wagner and Boyce, 2003), the commonly Sb-bearing quartz veins appear to be related to late stages of the Variscan orogeny (310–280 Ma). Hence, the hydrothermal deposits of the Schwarzwald area have been classified into Variscan Sb–($\pm$Ag $\pm$ Bi $\pm$ Au)–quartz veins and post-Variscan fluorite–barite–quartz veins. Most of the post-Variscan veins do not host minerals suitable for radiometric dating. For some of these veins such as Badenweiler, however, a Tertiary age is proven by their occurrence on the Rhine Graben boundary fault, which is of Tertiary age. For the other veins, the isotopic dating of pitchblende (U–Pb and U–Xe, Xe–Xe), primary hematite (U–He), and K-bearing minerals (K–Ar) revealed three mineralization events. The first was dated at 310–280 Ma, at the end of the Variscan orogeny (Hofmann and Eikenberg, 1991; Segev et al., 1991; Meshik et al., 2000; Wittichen area, Menzenschwand deposit), a second one at 150–110 Ma (Segev et al., 1991; Wernicke and Lippolt, 1993; Wernicke and Lippolt, 1997; Hohberg and Eisenbach area), and a third one at 50–30 Ma related to the formation of the Rhine Graben structure (Hofmann and Eikenberg, 1991; Menzenschwand deposit). K–Ar

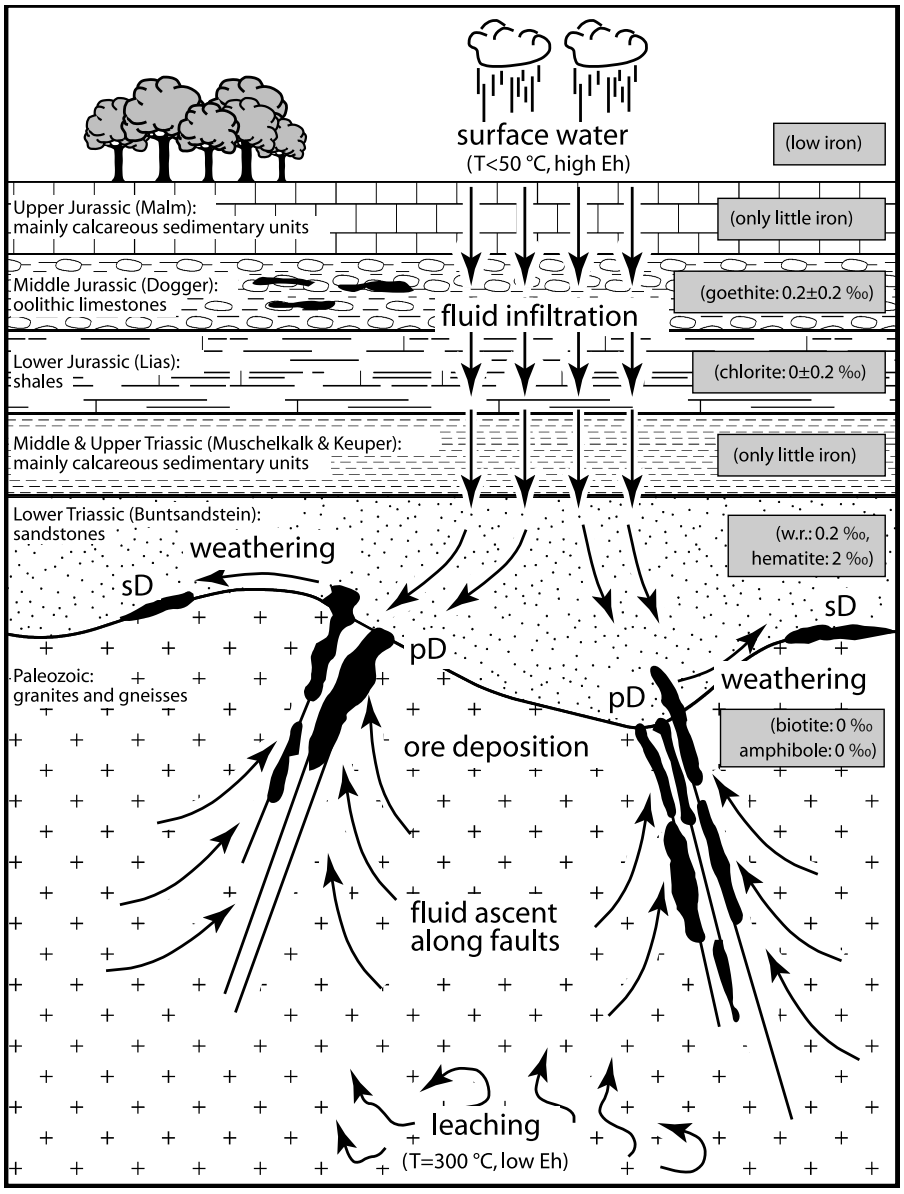

Fig. 2. Iron reservoirs and their respective iron isotope ratios relevant for ore-forming and alteration processes in the Schwarzwald region. Primary Fe deposits (pD): fluid mixing and precipitation of siderite (intermediate Eh, $\Delta_{\text{sid–Fe(II)aq}} = -1.5‰$ to $-0.5‰$) or hematite (high Eh, $\Delta_{\text{hem–Fe(II)aq}} = +1.5‰$), $T = 100$–200 °C. Secondary Fe deposits (sD): weathering and dissolution (high Eh, $\Delta_{\text{Fe(II)aq–silicate}} = -1.2‰$ to $-0.1‰$), reprecipitation within deposit (high Eh, $\Delta_{\text{goethite or hematite–Fe(II)aq}} = +1.5‰$), $T = 100$–200 °C. Note that Δ is the difference between product and precursor.

and Ar–Ar dates of sericitized feldspars from the basement and the overlying Triassic Buntsandstein sandstone are in the range 150–110 Ma (Lippolt and Kirsch, 1994; Zuther and Brockamp, 1988; Meyer et al., 2000), which correlates well with the second hydrothermal event.

It is clear from the geological and metallogenic framework that the Schwarzwald iron ore deposits formed discontinuously over a large age range. As a consequence, they contain both primary and secondary iron minerals. These are distinguished from each other based on their textures. Primary iron minerals (hematite, siderite) are between 1 and 20 mm in size. They typically consist of large euhedral crystals, intergrown with primary gangue minerals such as barite or quartz or grown directly onto the host rocks (Fig. 3a–c). The primary siderite was partly oxidized at high temperatures and a secondary high-temperature hematite formed. Hence, the primary iron minerals were redeposited either locally or into a more distant deposit by secondary processes. Temperatures were high (>100 °C) during this alteration. Later supergene (i.e., low temperature) weathering after partial or complete erosion of the sedimentary cover led to decomposition and oxidation of the primary siderite. During this process, botryoidal goethite or hematite (''glaskopf'', Fig. 3d–f) or very fine-grained hematite as thin, reddish leaf-style crystals were formed at pressures and temperatures close to those prevailing at the surface (sD on Fig. 2). The complete replacement of siderite is indicated by a residue comprising

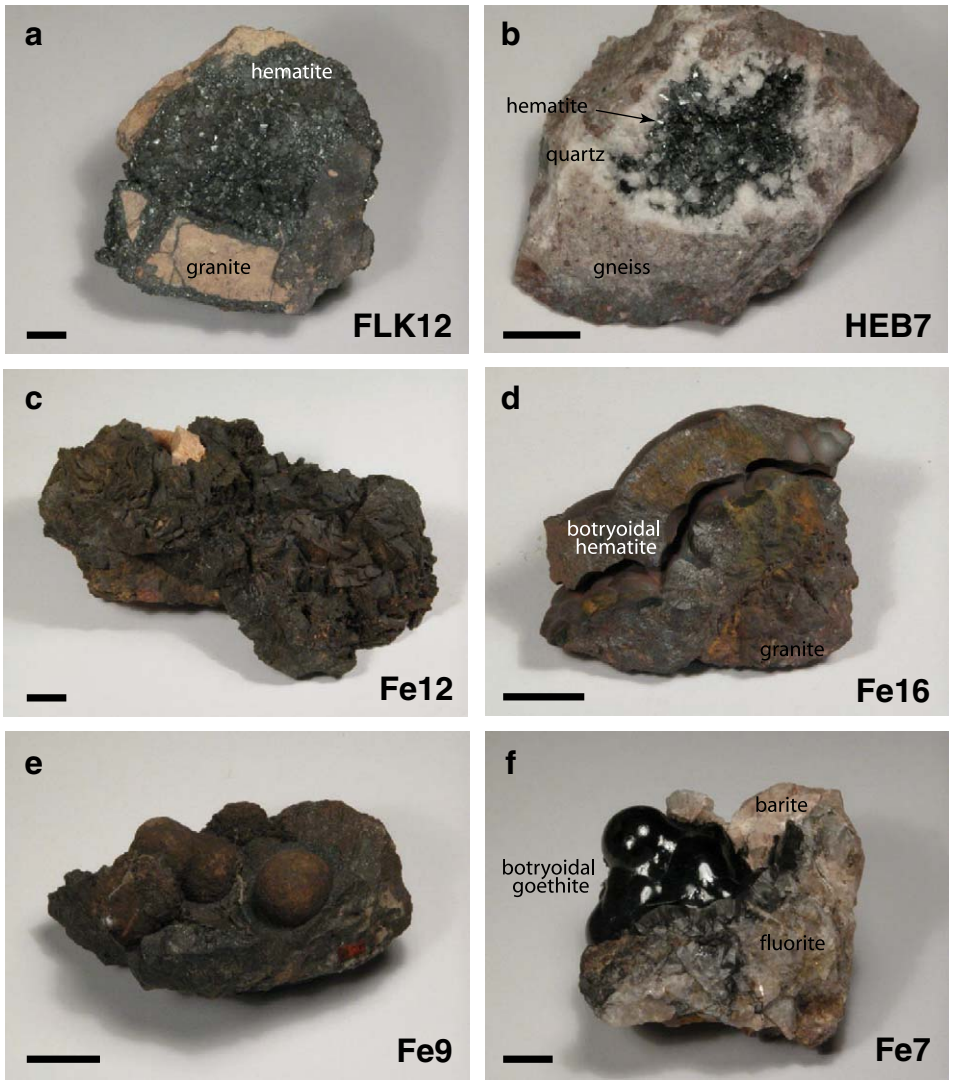

Fig. 3. Photographs of some typical iron ore samples. (a) Fresh, euhedral, primary hematite crystals on a granite breccia from Lenzkirch (sample FLK 12). (b) Fresh hematite crystals in a quartz vug from Erlets near Hausach (sample HEB7). (c) Dark brown, partly oxidized siderite crystals from Neuenbürg (sample Fe12). (d) Fibrous secondary hematite (''red glaskopf'') from the Rappenloch mine (sample Fe16). (e) Botryoidal secondary goethite (''brown glaskopf''), Neuenbürg (sample Fe9). (f) Fibrous, glossy secondary goethite (''brown glaskopf''), Clara mine (sample Fe7). Scale bar is 1 cm.

either hollow pseudomorphs or dark brown crystal relicts, which now consist of Fe(III)-oxides and -hydroxides (mainly goethite). In the following, we will use the terms primary (high-temperature hematite and siderite of first generation), secondary (high-temperature hematite of second generation) and alteration or weathering assemblage (low-temperature mineralization).

3. Sampling strategy and sample description

This study combines samples from the entire area of the Schwarzwald district and its surroundings, from various types of iron mineral-bearing veins and from Fe-bearing Mesozoic sediments. The iron ores were formed in a period spanning more than 200 Ma of formation history. The sample locations are displayed on Fig. 1 and the samples are briefly described in Table 1. The following types of samples were investigated:

(1) Primary iron minerals (crystalline hematite (FeIII; Fig. 3a and b), chalcopyrite (FeIII), siderite (FeII; Fig. 3c) and pyrite (FeII)) from hydrothermal veins. The hydrothermal veins occur exclusively in the Schwarzwald basement and in the Buntsandstein cover sequence at the eastern border of the Schwarzwald. They do not penetrate the other overlying sedimentary strata.
(2) On a few samples, partial oxidation processes of the primary siderite at high temperatures led to the formation of crystalline, secondary hematite. Based on textures such as in sample M590, in which microcrystalline hematite is ''sandwiched'' between two generations of high-temperature siderite, this secondary hematite definitely formed at higher temperatures.
(3) Supergene iron minerals include the Fe(III)-arsenates Ba-pharmacosiderite and scorodite and in particular the Fe(III)-oxides and -hydroxides goethite and

Table 1
Samples, sample descriptions, location code for Fig. 1a, and measured iron isotope values from Schwarzwald iron minerals and ores

Sample No.	No. on Fig. 1	Mineral	p/s	Locality	δ^{56}Fe	δ^{57}Fe	Sample description
					Mass-spectrometric duplicates; bold: sample average		
FE2	6	Siderite	p/s	Mine Clara, Wolfach	−0.80	−1.17	Dark brown, lensoid
					−0.80	−1.18	crystals, oxidized, in vug
					−0.80	**−1.18**	on barite
FE3	6	Siderite	p	Mine Clara, Wolfach	−0.99	−1.52	Light brown, radially
					−1.00	−1.53	aggregated, fresh crystals
					−0.99	**−1.52**	up to 5 mm, on barite, overgrown by calcite and hematite
M420	7	Siderite	p/s	Mine Sophia, Wittichen	−0.86	−1.27	Dark brown, oxidized,
					−0.85	−1.27	rhombohedral crystals in
					−0.85	**−1.27**	vug on barite crystals
M590	7	Siderite I	p	Mine Sophia, Wittichen	**−1.36**	**−2.01**	First generation, coarse-grained, anhedral siderite on barite
M590	7	Siderite II	p	Mine Sophia, Wittichen	−0.74	−1.07	Fresh rhombohedral
					−0.75	−1.17	crystals on small
					−0.74	**−1.12**	hematite crystals which overgrown an earlier generation of siderite
FE10	1	Siderite	p/s	Neuenbürg	−0.86	−1.24	Dark brown oxidized
					−0.80	−1.21	crystals on barite
					−0.83	**−1.23**	
FE12	1	Siderite	p/s	Neuenbürg	−0.73	−1.05	Oxidized, dark brown
					−0.72	−1.03	rhombohedral crystals
					−0.72	**−1.04**	on sandstone
WEIN2202	6	Chalkopyrite	p	Mine Clara, Wolfach	−0.34	−0.45	Fresh, golden, anhedral
					−0.32	−0.48	masses in barite
					−0.33	**−0.47**	
		Repeat dissolution			−0.25	−0.43	
					−0.32	−0.47	
					−0.28	**−0.45**	
WEIN2202	6	Pyrite	p	Mine Clara, Wolfach	−0.29	−0.46	Fresh, golden crystals in
					−0.26	−0.41	and with chalcopyrite
					−0.28	**−0.44**	
FE14	5	Chalcopyrite	p	Mine Friedrich-Christian, Wildschapbach	−0.30	−0.40	Fresh, golden mass in
					−0.33	−0.44	quartz
					−0.32	**−0.42**	
FE14	5	Pyrite	p	Mine Friedrich-Christian, Wildschapbach	0.01	0.02	Fresh, golden crystals in
					−0.03	0.01	and with chalcopyrite in
					−0.01	**0.02**	quartz
Fe5	6	Ba-pharmacosiderite	s	Mine Clara, Wolfach	−0.20	−0.27	2 mm large brown cubic
					−0.13	−0.18	crystals on barite
					−0.16	**−0.22**	
FE6	6	Scorodite	s	Mine Clara, Wolfach	−0.21	−0.33	3 mm large bluish
					−0.26	−0.40	crystals on
					−0.24	**−0.37**	pseudomorphed chalcopyrite
Fe1-1	17	Hematite	p	Mine Rappenloch, Eisenbach	−0.29	−0.43	Relatively large, fresh
					−0.27	−0.43	crystals
					−0.28	**−0.43**	
Fe4-1	8	Hematite	sh	Mine Anton, Heubach near Wittichen	0.83	1.23	Small, free, euhedral
					0.91	1.35	crystals, very thin, red, in
					0.87	**1.29**	barite vugs
		Repeat dissolution			0.83	1.19	
					0.79	1.17	
					0.81	**1.17**	
Fe5-1	1	Hematite	s	Neuenbürg	−0.44	−0.66	Layer of red, feathery
					−0.44	−0.66	crystals
					−0.44	**−0.66**	

Table 1 (*continued*)

Sample No.	No. on Fig. 1	Mineral	p/s	Locality	δ^{56}Fe	δ^{57}Fe	Sample description
FE3	6	Hematite	s	Mine Clara, Wolfach	−0.62	−0.89	Small, red, thin crystals
					−0.70	−1.03	in vugs on siderite,
					−0.66	**−0.96**	together with calcite
FLK12	18	Hematite	p	Lenzkirch	0.40	0.61	Large, fresh, euhedral crystals up to 1 cm on granite porphyry
FE1	19	Hematite	p	Sirnitz, Münstertal	−0.49	−0.74	Fresh, euhedral crystals up to 2 mm on quartz-cemented granite breccia
FLK20	18	Hematite	p	Lenzkirch	0.08	0.10	Large euhedral crystals
					0.06	0.10	on granite porphyry,
					0.07	**0.10**	very slightly oxidized
FE4	6	Hematite	sh	Mine Clara, Wolfach	0.89	1.33	2 mm large tabular
					0.91	1.28	crystals on quartz
					0.90	**1.30**	
M590	7	Hematite	sh	Mine Sophia, Wittichen	0.85	1.16	Very tiny, red, free
					0.77	1.09	crystals, on earlier and
					0.81	**1.13**	below later generation of siderite
FE8	3	Hematite	s	Kienberg near Freudenstadt	−1.06	−1.65	Layer of red feathery
					−1.10	−1.63	crystals on fibrous
					−1.08	**−1.64**	goethite
PHB4	9	Hematite	s	Hohberg, St. Roman	−1.48	−2.19	Outermost layer of 3 cm
					−1.52	−2.31	thick fibrous, radial
					−1.50	**−2.25**	hematite (“red glaskopf”)
PHB4	9	Hematite	s	Hohberg, St. Roman	−0.58	−0.83	Innermost core layer of
					−0.58	−0.81	3 cm thick fibrous, radial
					−0.58	**−0.82**	hematite (“red glaskopf”)
METZ557	13	Hematite	p	Mine Eisenwand, Zell a. H.	0.08	0.16	Layer of up to 6 mm
					0.08	0.09	large crystals in quartz
					0.08	**0.12**	
HEB7	11	Hematite	p	Erlets near Hausach	0.42	0.55	Up to 5 mm large single
					0.41	0.59	crystals in quartz vug
					0.41	**0.57**	
FE9	1	Hematite	s	Neuenbürg	−0.24	−0.34	Layer of red, feathery
					−0.25	−0.35	crystals
					−0.24	**−0.35**	
FE11	12	Hematite	p	Mine Otto, Schottenhöfe, Zell a. H.	0.31	0.46	Up to 5 mm large, fresh,
					0.30	0.44	euhedral crystals on
					0.30	**0.45**	microcrystalline hematite
FE11	12	Hematite	s	Mine Otto, Schottenhöfe, Zell a. H.	−0.98	−1.47	Microcrystalline, dense
					−0.97	−1.43	hematite on barite
					−0.97	**−1.45**	
FE13	10	Hematite	s	Streckfeld near Wolfach	−1.15	−1.68	Layer of red, feathery
					−1.17	−1.75	crystals on goethite
					−1.16	**−1.72**	
GMS04	20	Hematite	p	Menzenschwand	−0.04	−0.07	Large, fresh, euhedral crystals in vug on granite
FE15	17	Hematite	p	Mine Rappenloch, Eisenbach	0.06	0.09	Layer of up to 5 mm
					0.03	−0.02	large, fresh crystals
					0.04	**0.03**	
FE15	17	Hematite	p	Mine Rappenloch, Eisenbach	−0.10	−0.17	Fresh, microcrystalline
					−0.13	−0.18	layer
					−0.11	**−0.18**	
FE16	17	Hematite	s	Mine Rappenloch, Eisenbach	−0.80	−1.15	Fibrous crystals (“red
					−0.76	−1.10	glaskopf”), layered
					−0.78	**−1.12**	
FE17	16	Hematite	p	Farrenberg near Eisenbach	0.03	0.04	Layer of up to 3 cm
					0.00	−0.01	large, fresh crystals on
					0.01	**0.01**	granite

(*continued on next page*)

Table 1 (*continued*)

Sample No.	No. on Fig. 1	Mineral	p/s	Locality	δ^{56}Fe	δ^{57}Fe	Sample description
FE18	14	Hematite	p	Lägerfelsen, Triberg	−0.30	−0.43	Layer of crystals up to
					−0.28	−0.43	5 mm on rhyolite
					−0.29	**−0.43**	
FE19	15	Hematite	p	Fahlenbach near	0.56	0.81	Feathery crystals in
				Eisenbach	0.50	0.78	barite on granite
					0.53	**0.79**	
FE20	2	Goethite	s	Mine Schrotloch,	−0.80	−1.18	Fibrous crystals (“brown
				Hornisgrinde	−0.81	−1.20	glaskopf”)
					−0.81	**−1.19**	
FE21	1	Goethite	s	Neuenbürg	−0.64	−0.93	Fibrous crystals (“brown
					−0.64	−0.96	glaskopf”)
					−0.64	**−0.94**	
Fe7	6	Goethite	s	Mine Clara, Wolfach	−0.80	−1.22	Fibrous mass (“brown
					−0.80	−1.21	glaskopf”), shiny black
					−0.80	**−1.21**	on the surface, fibres up
							to 5 mm long
QFS26	4	Goethite	s	Mine Dorothea,	−0.51	−0.70	Fibrous mass (“brown
				Freudenstadt	−0.56	−0.76	glaskopf”), fibres up to
					−0.53	**−0.73**	2.5 cm long
		Repeat			−0.50	−0.76	
		dissolution			−0.48	−0.74	
					−0.49	**−0.75**	
WEIN2321	12	Goethite	s	Mine Otto,	−1.13	−1.68	Fibrous goethite
				Schottenhöfe, Zell a. H.	−1.11	−1.63	(“brown glaskopf”) on
					−1.12	**−1.66**	barite
FE8	3	Goethite	s	Kienberg near	−0.52	−0.82	Fibrous, brown
				Freudenstadt	−0.53	−0.78	glaskopf, below hematite
					−0.52	**−0.80**	
Fe2-1	24	Goethite		Donaueschingen, E of	0.00	−0.02	1 mm large oolites from
				Schwarzwald	0.04	0.07	sedimentary iron ore
					0.02	**0.02**	
Fe3-1	23	Goethite		Kandern, W of	−0.01	−0.01	1 mm large oolites from
				Schwarzwald	0.01	0.04	sedimentary iron ore
					0.00	**0.01**	
FE22	26	Goethite		Geisingen, Baar, E of	0.02	0.05	1 mm large oolites from
				Schwarzwald	0.01	0.04	sedimentary iron ore
					0.05	0.06	
					0.11	0.17	
					0.05	**0.08**	
FE23	25	Goethite		Achdorf, Wutach E of	0.44	0.63	1 mm large oolites from
				Schwarzwald	0.41	0.61	sedimentary iron ore
					0.42	**0.62**	
FE24	21	Goethite		Ringsheim near Lahr, W	0.06	0.03	1 mm large oolites from
				of Schwarzwald	0.06	0.06	sedimentary iron ore
					0.06	**0.04**	
FE25	22	Goethite		Schliengen S Freiburg,	0.28	0.38	1 cm large oolites from
				W of Schwarzwald	0.31	0.43	sedimentary iron ore
					0.30	**0.41**	
FE26	27	Goethite		Thalheim near	0.27	0.35	1 mm large oolites from
				Tuttlingen, E of	0.31	0.44	sedimentary iron ore
				Schwarzwald	**0.29**	**0.39**	
FE27	23	Goethite		Kandern S Freiburg, E	0.09	0.07	1 cm large oolites from
				of Schwarzwald	0.11	0.14	sedimentary iron ore
					0.10	**0.10**	
FE28		Sandstone		Schramberg	**0.22**	**0.35**	Whole-rock analysis,
							brick-red, fine-grained
							sandstone
FE29		Shale		Dotternhausen	**−0.21**	**−0.28**	Whole-rock analysis,
							Lias ε, black shale
FE32		Shale		Holzmaden	**0.03**	**0.04**	Whole-rock analysis,
							Lias ε, black shale

p denotes primary minerals, s secondary minerals formed under supergene conditions and sh denotes secondary minerals formed at higher than supergene temperatures.

hematite, the latter two in their fibrous form (“glaskopf”, Fig. 3d–f). All these phases formed by weathering and oxidation of the primary iron ores in the hydrothermal veins. In some cases, the secondary minerals are pseudomorphs that formed by in situ replacement of the primary minerals. In other cases, the iron was transported over some millimeters, centimeters or meters before it was re-precipitated. Hence, the secondary minerals occur both directly on the relicts or close to the relicts of the primary ones. In Table 1, minerals separated from the same hand specimen are indicated by a common sample number. They were typically sampled millimeters to a few centimeters from each other.

(4) Iron-bearing sediments from the Buntsandstein, the Lias and the Dogger were analyzed to constrain the variations in Fe isotope composition of the sedimentary cover sequence, which may have acted as source of Fe for some of the post-Variscan veins in the basement (Fig. 2). The Dogger sediments are coastal oolithic limestones which host large amounts of iron-oxides and -hydroxides. Their depositional age overlaps with the radiometric ages of some of the massive hydrothermal hematite veins in the Schwarzwald.

4. Analytical procedures and results

4.1. Analytical procedures

From all samples except the sedimentary oolitic iron ores, of which whole-rock powders were used, hand-picked mineral separates were used for analysis. All measurements were performed at the geochemistry laboratory of the University of Hannover. The analytical method is explained in detail by Schoenberg and von Blanckenburg (2005), and is only briefly repeated here. Mineral separates were first decomposed in 6 M HCl. Iron was separated from the mineral matrix by anion exchange chromatography and checked for purity by ICP-OES. Isotope measurements were performed on a ThermoFinnigan Neptune instrument using the sample-standard-sample bracketing technique. A detailed description of the chemical and mass-spectrometric procedures is presented by Schoenberg and von Blanckenburg (2005). They found that the overall 95% confidence interval reproducibility is ±0.049‰ (δ^{56}Fe) and 0.071‰ (δ^{57}Fe). The isotope data shown in Table 1 contain both mass-spectrometric duplicates (repeat analyses of the same purified Fe aliquot) and real sample duplicates (repeat decompositions of separate sample powders). The mass-spectrometric duplicates reproduce within the ranges given above, while repeat decompositions might exhibit sample heterogeneity. This issue will be addressed elsewhere, but samples from Hohberg (PHB4) and Rappenloch (Fe15 and Fe16) give an indication of heterogeneity within and between samples. All isotope ratios are reported relative to the IRMM-14 Fe isotope standard. The $^{56}Fe/^{54}Fe$ ratio has been converted into δ^{56}Fe according to

$$\delta^{56}\mathrm{Fe}_{\mathrm{sample}} = \left(\frac{{}^{56}\mathrm{Fe}/{}^{54}\mathrm{Fe}_{\mathrm{sample}}}{{}^{56}\mathrm{Fe}/{}^{56}\mathrm{Fe}_{\mathrm{IRMM\text{-}14}}} - 1 \right) \times 100$$

and the δ^{57}Fe likewise.

4.2. Results

The iron isotope compositions are listed in Table 1 and displayed in Fig. 4. The δ^{56}Fe values vary between about −1.5‰ and +0.9‰, hence over almost 2.5 delta units. The isotope ratios are distinct between and within mineral groups. They are also different and much more variable than the +0.04% to +0.38% range (relative to IRMM-14)

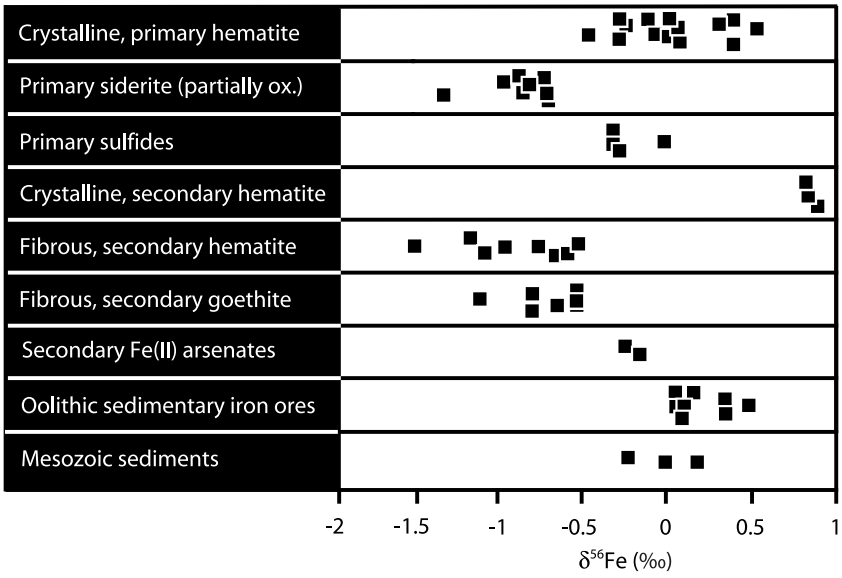

Fig. 4. Iron isotopic compositions of primary and secondary iron minerals from hydrothermal veins, and of sediments from the Schwarzwald area.

found for igneous rocks (Beard et al., 2002; Poitrasson and Freydier, 2005) or the −0.2‰ to +0.3‰ range found for clastic sediments and river suspended loads (Beard and Johnson, 2004).

4.2.1. Primary and secondary oxidic iron minerals from hydrothermal veins

Large variations of their δ^{56}Fe values were measured in both primary and secondary Fe(III)-oxides and -hydroxides (goethite and hematite). Primary hematite crystals have δ^{56}Fe values between −0.49‰ and +0.53‰, whereas secondary hematite displays two sample groups: hematite formed during supergene alteration (group "s" in Table 1) contains light iron throughout with δ^{56}Fe values between −1.5‰ and −0.58‰, while secondary hematite formed at high temperatures (group "sh" in Table 1) shows δ^{56} Fe between +0.81‰ and +0.9‰. Within one-layered fibrous hematite sample (Fig. 3d), δ^{56}Fe values vary over a distance of about 3 cm from core to rim between −0.58‰ and −1.5‰ (sample PHB 4 in Table 1). Fibrous goethite ranges between −1.12‰ and −0.51‰, very similar to low-T hematites.

4.2.2. Primary and secondary non-oxidic iron minerals from hydrothermal veins

Pyrite, chalcopyrite and siderite show relatively small variations in their iron isotopic compositions, but exhibit large differences to other minerals from the same vein. Coexisting pyrite and chalcopyrite from the Clara deposit have indistinguishable iron isotopic compositions of about δ^{56}Fe = −0.30‰, whereas samples from the Friedrich-Christian deposit show a difference between pyrite (δ^{56}Fe = −0.01‰) and chalcopyrite (−0.32‰). The chalcopyrite value is almost identical in both deposits. The siderites from three different deposits (including the Clara deposit) have δ^{56}Fe values in the range between −1.36‰ and −0.72‰; the Clara siderites contain iron with δ^{56}Fe of −1.0‰ (fresh siderite) and −0.8‰ (slightly oxidized to goethite). A similar pattern is observed at Neuenbürg, where the δ^{56}Fe value of fresh siderite is −0.83 while that of the oxidized sample is −0.72‰. Three samples from the Sophia mine near Wittichen show δ^{56}Fe of −1.36‰ (fresh siderite I), −0.72‰ (fresh siderite II) and −0.85‰ (slightly oxidized siderite, probably of a second generation). Small variations between −0.16‰ and −0.24‰ are displayed by the secondary Fe(III)-arsenates Ba-pharmacosiderite and scorodite, of which, however, only two samples were analyzed.

4.2.3. Sediments

Relatively small variations are observed in goethite from the Dogger oolitic iron ores, with δ^{56}Fe values being between +0.02‰ and +0.42‰. The range indicates that the iron source of these sediments was rather homogeneous and that the isotope fractionation during low-temperature precipitation was similar in coastal environments over relatively large distances (the samples were deposited 50 km apart from each other).

In addition to the oolitic Dogger ores, three whole-rock samples of iron-bearing Mesozoic sediments from the Schwarzwald area have been analyzed. While a Buntsandstein (sandstone, sample FE28) has a δ^{56}Fe value of +0.22‰, two black shales from the Schwäbische Alb (samples FE29 and FE32) have values of −0.21 and 0.03, respectively. Hence, the shales show similar isotopic variations—but shifted to slightly lighter δ^{56}Fe values—as the oolitic Dogger ores. Overall, the δ^{56}Fe range measured in sediments is within the range observed for modern clastic marine sediments (−0.2‰ to +0.3‰, Beard and Johnson, 2004). Basement granites and gneisses from the study area have not been analyzed for their Fe isotopic composition, but in general, crystalline basement rocks have δ^{56}Fe values around +0.1‰ to 0.38‰ (Beard et al., 2002; Poitrasson and Freydier, 2005).

5. Thermodynamic modelling of iron leaching, precipitation and alteration

The data indicate that various processes contribute to the change in iron isotope compositions. In principle, three stages can be distinguished, during which fractionation can occur, which are leaching, precipitation and supergene alteration. Considering that redox reactions play an important role during these processes, particularly for iron isotope fractionation, we have thermodynamically modeled various reaction parameters and iron speciation during (1) leaching of iron from crystalline basement rocks through fluid–rock interaction (Figs. 5 and 6), (2) precipitation of Fe minerals through fluid mixing in the vein deposits (Fig. 7), and (3) supergene weathering of siderite through interaction with oxidizing surface-derived waters (Fig. 8). This involved calculations of phase diagrams and various reaction path simulations in the model system Na–K–Ca–Fe–Al–Si–C–Cl–O–H and several subsystems. We have not included sulfur into the model system for two main reasons. First of all the solubility of Fe in hydrothermal fluids with high salinities is mostly controlled by Cl complexes. The concentration of sulfur is several orders of magnitude smaller, resulting in only a subordinate control on Fe solubility. Second, no reliable thermodynamic data for reduced Fe–S species such as $Fe(HS)^+$ or $Fe(HS)_2$ are available and there are only data for one oxidized Fe–S species, the $FeSO_4^0$ complex.

5.1. Setup of the thermodynamic model

The calculations were carried out with the HCh software package (Shvarov and Bastrakov, 1999), which models heterogeneous equilibria and reaction progress by minimization of the Gibbs free energy of the total system (Shvarov, 1978, 1981). This package contains an extensive data management facility, which allows efficient calculation of the thermodynamic properties of mineral-fluid reactions.

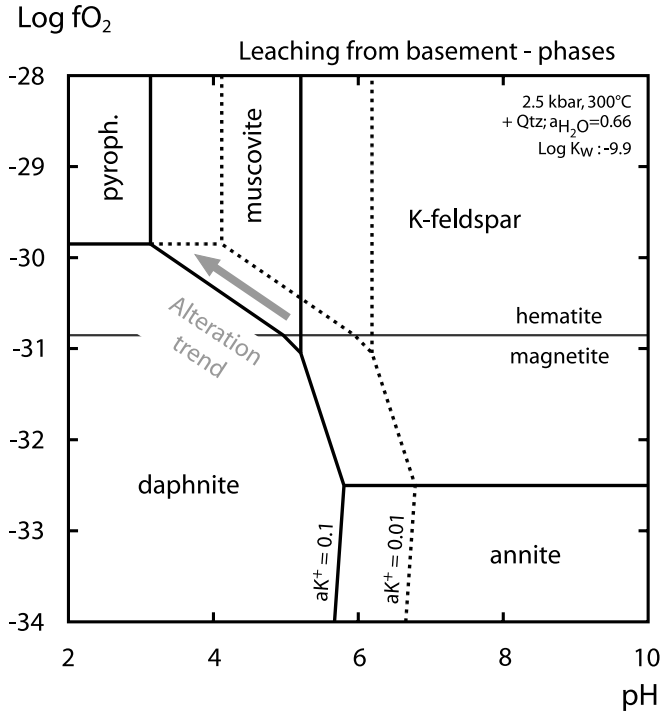

Fig. 5. The log f_{O_2}—pH diagram constructed at 300 °C, 2.5 kbar and an H_2O activity of 0.66, showing mineral stability relationships in the system K–Fe–Si–Al–O–H. The thin solid line shows the magnetite–hematite transition, whereas the thick solid and thick dotted lines delineate stability fields of silicate minerals at activities of K^+ of 0.1 and 0.01, respectively. The alteration trend (grey arrow) indicates the concurrent change in pH and oxidation state via progressive hydrothermal alteration (transition from rock-buffered to fluid-buffered conditions) of the basement granites/gneisses. Note that at 300 °C and 2.5 kbar the neutral point corresponds to a pH of 4.95.

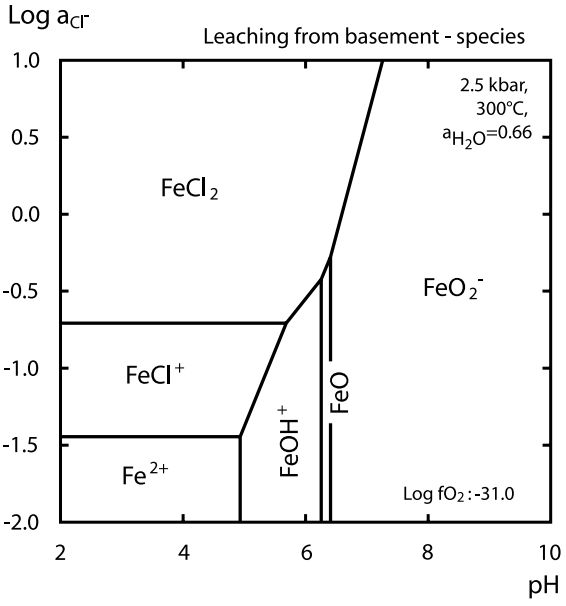

Fig. 6. Predominance diagram of aqueous Fe species in pH—log a_{Cl^-} space, constructed at 300 °C, 2.5 kbar and an H_2O activity of 0.66. The log f_{O_2} was fixed at −31, which conforms to the lower endpoint of the alteration trend (see Fig. 5). Increasing the log f_{O_2} to −30 (upper endpoint of the alteration trend) essentially results in the same topology, with only the field of FeO disappearing. At the conditions of hydrothermal fluid–rock interaction in the basement of the Schwarzwald district, $FeCl_2$ is by far the predominant aqueous Fe species. Note that the stoichiometries of aqueous species are given in the notation used by Shock et al. (1997).

Thermodynamic data for aqueous species were essentially taken from the SUPCRT92 database and subsequent updates (Johnson et al., 1992; Shock et al., 1997; Sverjensky et al., 1997), with additional data for several aluminum species from Tagirov and Schott (2001). Thermodynamic data for silicate, oxide, hydroxide and carbonate minerals were taken from the internally consistent dataset of Holland and Powell (1998). All calculations of individual activity coefficients of aqueous species applied an extended Debye-Hückel model using the b-gamma equation for NaCl as the background electrolyte (Oelkers and Helgeson, 1990; Shock et al., 1992).

For the calculation of fluid–rock equilibria, whole-rock analyses of typical granites from the Schwarzwald area (Emmermann, 1977) were used to constrain the bulk rock composition of the crystalline basement. This composition was then recalculated to the system Na–K–Ca–Fe–Al–Si–Cl–O–H, which represents a simplified model of the rock composition (excluding Ti and Mn). The starting composition of the brine end-member used in the fluid mixing calculations was obtained by equilibrating a fluid having total solute concentrations and major cation ratios (K/Na and Ca/Na) typical of the post-Variscan hydrothermal system in the Schwarzwald district (as derived from microthermometric and LA-ICP-MS data; Markl, unpubl. data) with this average granite at 300 °C and 2.5 kbar. Several different meteoric end-member fluid compositions were modeled by equilibrating pure water at 50 °C and 1 bar with (1) calcite, at pO_2 and pCO_2 constrained at atmospheric values, (2) calcite, at atmospheric pCO_2, and (3) calcite only. Simulations of the alteration of siderite assumed that the oxidizing surface-derived water was pure water at 30 °C and 1 bar, with the dissolved oxygen content constrained from equilibration with O_2 gas at atmospheric partial pressure.

5.2. Results of the calculations

5.2.1. Leaching of iron from crystalline basement rocks

Leaching of iron from the basement was modeled using a typical granitic assemblage of K-feldspar, quartz and two micas. At 2.5 kbar and 300 °C, K-feldspar is stable with either muscovite or biotite (annite) only (Fig. 5), but chlorite (daphnite) is a typical stable phase. At these conditions, a more-or-less neutral fluid (i.e., pH around 4.9) with realistic K^+ activities between 0.1 and 0.01 would be in the stability field of muscovite. Rock-buffering would move it to the invariant point defined by K-feldspar, chlorite (daphnite) and muscovite (plus quartz), where magnetite would be the stable iron oxide phase (Fig. 5). Through progressive fluid–rock interaction, slightly to strongly acidic and/or oxidized fluid batches penetrating the rock along previously reacted fractures would drive the fluid composition into the hematite stability field and would finally arrive at the

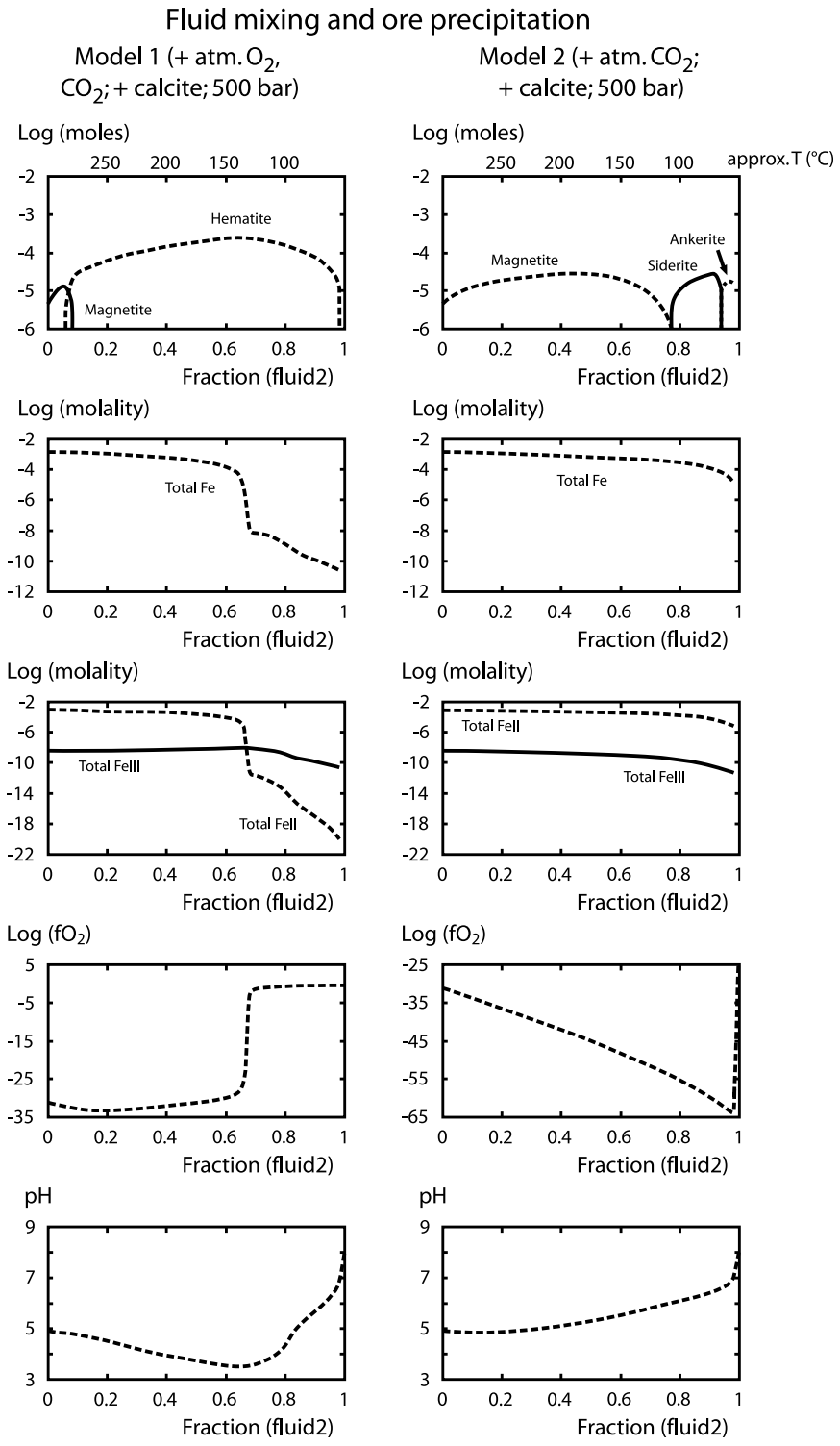

Fig. 7. Representative results of reaction path modeling for mixing of a deep saline brine (fluid1) with surface-derived meteoric water (fluid2). The starting composition of the brine end-member was obtained by equilibrating a fluid having total solute concentrations and major cation ratios (K/Na and Ca/Na) typical of the post-Variscan hydrothermal system with an average Schwarzwald granite at 300 °C and 2.5 kbar. The meteoric end-member chemistries were modeled by equilibrating pure water at 50 °C and 1 bar with calcite, at pO_2 and pCO_2 constrained at atmospheric values (model 1, left column), and calcite, at atmospheric pCO_2 (model 2, right column). The composition of the mixed fluid was then calculated as a function of the mass fraction of fluid2, defined as $m_{\text{fluid2}}/(m_{\text{fluid1}} + m_{\text{fluid2}})$, at a fixed pressure of 500 bar. It can be seen that in model 1 hematite is the stable iron phase formed throughout most of the simulation, whereas in model 2 magnetite is formed up to a mass fraction of fluid2 of about 0.75, where it is subsequently replaced by siderite and ankerite. The results of the simulations represent two end-member scenarios, which correspond to the two typical vein assemblages found in the Schwarzwald district.

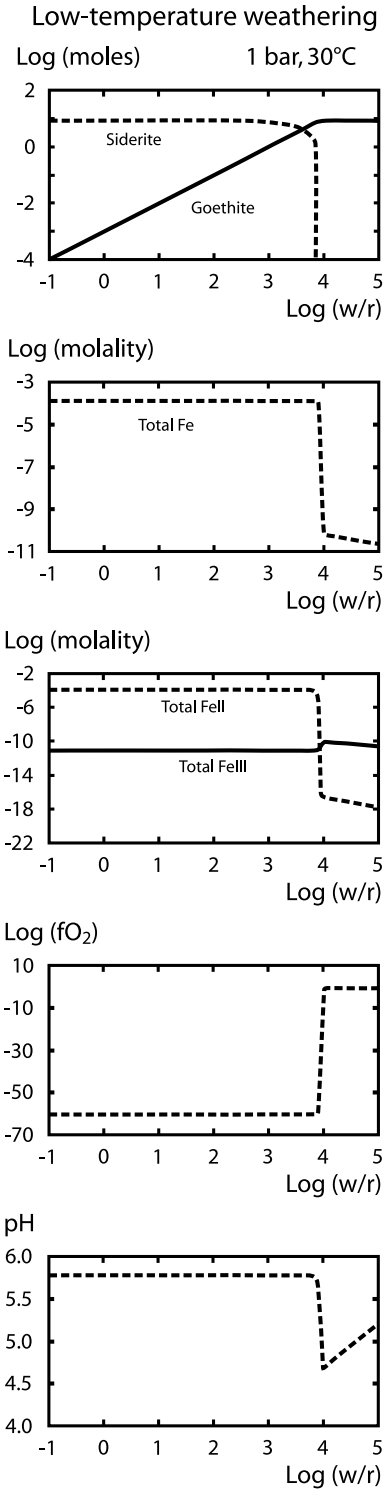

Fig. 8. Results of the simulation of weathering of siderite by surface-derived water at an increasing water/rock ratio. The calculations were performed assuming that the oxidizing surface-derived water was pure H_2O at 30 °C and 1 bar, with the dissolved oxygen content constrained by equilibration with O_2 gas at atmospheric partial pressure. The amount of goethite formed at the expense of siderite increases with increasing water/rock ratio until all siderite is consumed; this results in a sharp decrease of the total dissolved iron coupled with an increase in the oxidation state in the water.

invariant point defined by pyrophyllite, muscovite and daphnite (always plus excess quartz). This means that the system would evolve from rock- to fluid-buffered and during this evolution, where hematite would become the stable iron oxide phase in the rocks. This is indeed what is observed within alteration zones in the hydrothermally overprinted Schwarzwald granites.

A fluid having a composition between these two invariant points, i.e., along this alteration path, would have an iron speciation displayed in Fig. 6. At an oxygen fugacity of 10^{-31} bar and at acid to neutral pH, the dissolved iron is almost exclusively present in its divalent state. This picture does not change at slightly elevated f_{O_2} values (e.g., at an f_{O_2} of 10^{-30} bar only the stability field of the FeO aqueous species disappears, but the rest of the topology remains identical). Depending on chlorinity, Fe^{2+}, $FeCl^+$ or $FeCl_2$ are the dominant aqueous iron species. For the hydrothermal solutions responsible for granite alteration in the Schwarzwald, having high salinities between 20 and 40 wt% NaCl equivalent, $FeCl_2$ is the predominant aqueous iron species outweighing other species by about two orders of magnitude. Biotite or chlorite would be the main source of iron in the fluid and this, in turn, means that iron leached from the basement in 7–8 km depth and at 300 °C would be present as divalent iron in solution and no redox process would be involved during leaching.

5.2.2. Fluid mixing with surface water

This process is supported by a line of evidence presented by Schwinn et al. (2006). The hot, high-salinity hydrothermal fluid rises quickly from 7 to 8 km depth to a depth of about 1.5 km, where the actual precipitation of the hydrothermal minerals occurs by mixing with an oxidized surface-derived meteoric water of low temperature. The solubility of Fe(II) strongly depends on chlorinity of the fluid and on temperature (Seward and Barnes, 1997; Wood and Samson, 1998; Yardley, 2005). Hence, dilution of the highly saline brine by low-salinity surface water would provide a plausible mechanism for iron ore precipitation. However, redox effects may be involved in such precipitation processes. Therefore, the mixing process is modeled for two end-member scenarios, an oxidized one (left column in Fig. 7; surface water in equilibrium with atmospheric oxygen) and a reduced one (right column in Fig. 7; surface water not in equilibrium with atmospheric oxygen; f_{O_2} is buffered by H_2O dissociation only). It is obvious that a fluid in equilibrium with calcite (i.e., reacted with the Mesozoic sediments covering the Schwarzwald) and atmospheric O_2 and CO_2 will precipitate mostly hematite during this mixing process. The Fe(II)/Fe(III) ratio changes from Fe(II)-dominated in the deep, hot fluid to Fe(III)-dominated in solutions with a significant proportion of meteoric water. The total iron content drastically drops at a mixing ratio of about 0.7 (brine/meteoric). Interestingly, the fluid mixture has a temperature of 120–150 °C at this point, which conforms to the mode of fluid inclusion homogenization temperatures in the Schwarzwald veins.

The precipitation process of the relatively reduced fluid is completely different. At high-brine/meteoric fluid ratios, magnetite would precipitate, while at fluid compositions dominated by the meteoric fluid, siderite and ankerite form instead. Their formation is not predicted for the oxidized case, which indicates that the commonly observed siderite in the later stages of the Schwarzwald hydrothermal veins was formed from more reduced and/or CO_2-enriched fluids. This mixing process is much less effective in precipitating the iron and the Fe(II)/Fe(III) ratio is always dominated by Fe(II). The pH curves for both mixing models are very similar. The models show that in the hematite-bearing veins significant oxidation occurs during the precipitation process, whereas no oxidation occurs during precipitation of siderite. While a homogeneous source for the deep fluid can be inferred, the meteoric fluid is most probably of slightly to strongly variable composition. Its oxidation state may be dependent on possible interactions with organic-rich black shale sediments in the Mesozoic cover sequence of the Schwarzwald and the depth of the equilibration with the host rocks (at oxic or anoxic conditions).

5.2.3. Supergene weathering of siderite deposits

Low-temperature alteration of iron-bearing ore deposits is a final process which can result in the fractionation of iron isotopes. Specifically, we have modeled supergene alteration of a siderite deposit through reaction with oxidizing surface-derived water at increasing water/rock (w/r) mass ratios (Fig. 8), i.e., at each step a fixed amount of fresh siderite was equilibrated with an increasing amount of the aqueous solution. This appears applicable to quite a number of veins in the northern and central Schwarzwald (e.g., Neuenbürg, Freudenstadt, Otto mine). In most of these deposits, earlier siderite is almost completely replaced by botryoidal hematite or goethite. With increasing water/rock ratio, the amount of goethite formed at the expense of siderite steadily increases until all siderite is consumed; this occurs at a log(w/r) of about 3.9 (Fig. 8). As long as both siderite and goethite are stable, the total dissolved Fe concentration, the Fe(II)/Fe(III) ratio, the oxygen fugacity and pH are buffered by this two-phase assemblage and remain constant. Total consumption of the siderite results in a very sharp transition, which is characterized by a decrease of the total dissolved Fe concentration by about 6 orders of magnitude, an increase in oxygen fugacity coupled with a decrease in the Fe(II)/Fe(III) ratio, and a decrease of the pH from about 5.8 to 4.7 (Fig. 8). With further increase of the water/rock ratio, the total dissolved Fe concentration decreases slightly, reflecting the effect of progressive dilution of the weathering solution. If similar calculations are performed at temperatures above 55 °C at atmospheric pressure, hematite substitutes goethite as the reaction product.

In summary, the results of the thermodynamic calculations demonstrate that iron isotope fractionation governed by redox reactions is likely to occur during the precipitation and the alteration processes, but not during high-temperature leaching of iron from the basement. We will now proceed to summarize the isotope fractionation effects relevant to these processes. A prerequisite to this effort is an inventory of the essential iron isotope fractionation factors relevant to these processes that have been published to date.

6. Iron isotope systematics

6.1. Iron isotope fractionation factors

The determination of fractionation factors for iron is, as for all other transition metal isotopes, still in its infancy. The available data are patchy and mostly not applicable to natural systems in a straightforward manner. The current status has recently been reviewed by Anbar (2004), and Johnson et al. (2004a). Basically, three independent approaches exist, which are (1) theoretical molecular partition functions, calculated from molecular and condensed-phase vibrational frequencies reviewed by Schauble (2004), (2) laboratory experiments under conditions that are as close as possible to those in nature, and (3) inferring empirical fractionation factors from natural observations. One of the principle obstacles in the experiments is establishing whether chemical equilibrium has been fully achieved, or whether measured isotope differences are due to kinetic effects (see review by Beard and Johnson, 2004). The empirical approach makes use of known mass fluxes, and known isotope ratios of influxes, effluxes and the compartments involved. Fractionation factors are calculated using Rayleigh-type mass balance equations. Often, natural isotope fractionation involves a series of fractionation steps, and only a cumulative fractionation factor is obtained that includes the sum of all steps. Here, the current status of fractionation factors relevant to this study is reviewed in detail. Rather than endorsing a particular fractionation factor it is deliberately left to the reader to assess the uncertainty introduced into the interpretation.

6.1.1. Fractionation among aqueous species

The most prominent and best-documented equilibrium fractionation factor is that of Fe(II) oxidation in aqueous Fe-containing solutions. Schauble et al. (2001) have determined a theoretical $\Delta_{Fe(III)aq–Fe(II)aq}$ value of +6‰ for the equilibrium reaction between the Fe(II)-hexaquo complex and the Fe(III)-hexaquo complex at 25 °C, and of +1.5‰ at 250 °C value ($\Delta_{product–reactand}$; here and in the following, the isotope fractionation $\Delta_{B–A}$ refer to the $^{56}Fe/^{54}Fe$ isotope ratio with A being the reactand compartment and B being the product compartment). These authors used vibrational spectroscopic data for a number of Fe complexes and an empirical force field model (Modified Urey-Bradley Force Field "MUBFF"). Anbar et al. (2005) have used Density Functional Theory ("DFT") and obtained $\Delta_{Fe(III)aq–Fe(II)aq}$ of +3.2‰ for the equilibrium reaction between the Fe(II)-hexaquo complex and the Fe(III)-hexaquo complex at 25 °C, and of +1.2‰ at 250 °C (Anbar et al.,

2005). The isotope fractionation between various Fe(III)-chloro complexes and the Fe(II)-hexaquo complex is predicted to be of the same direction, but smaller. For example, a δ value of 4‰ was predicted for the equilibrium reaction between $Fe(III)(H_2O)_4Cl_2^+$ complex and the Fe(II)-hexaquo complex at 25 °C, and of ca. 1‰ at 250 °C, respectively (Schauble et al., 2001). A fractionation of about half that magnitude was predicted for the reaction between $Fe(III)Cl_4^-$ and the Fe(II)-hexaquo complex (Schauble et al., 2001). Iron in the $FeCl_2$ complex is ca. 2‰ lighter than the Fe(II)-hexaquo complex at 25 °C, and ca. 1‰ lighter at 250 °C (Schauble et al., 2001). The oxidation of ferrous iron has been also calibrated in laboratory experiments, and the probably best-calibrated Fe fractionation factor resulted (reviewed by Beard and Johnson, 2004). The equilibrium reaction between the reactand $Fe(II)_{aq}$ and the product $Fe(III)_{aq}$ led to a $\Delta_{Fe(III)aq-Fe(II)aq}$ value of +2.9‰ at 25 °C (Welch et al., 2003). This fractionation factor is in excellent agreement with the DFT-derived theoretical value (Anbar et al., 2005), but it is half of that predicted by MUBFF (Schauble et al., 2001). This reaction has not yet been calibrated at higher temperatures...

6.1.2. Fluid–solid fractionation

Theoretical equilibrium fractionation factors using a combination of DFT (Anbar et al., 2005) and Mössbauer-derived (Polyakov, 1997) fractionation factors have been determined for the formation of hematite and goethite from the Fe(III)-hexaquo complex (Anbar et al., 2005). The $\Delta_{hematite-Fe(III)OOH}$ is −1.8‰ at 25 °C, and −0.6‰ at 250 °C, whereas the $\Delta_{goethite-Fe(III)OOH}$ is −3.5‰ at 25 °C, and ca. −1.3‰ at 250 °C, respectively. The light Fe isotope composition of hematite was experimentally predicted by Skulan et al. (2002). However, fractionation between $Fe(III)_{aq}$ and hematite is strongly reaction rate-dependent. At the fastest reaction rates the hematite was up to 1‰ lighter than the fluid, but when extrapolated to infinitely slow precipitation rates (assuming that this would present the equilibrium fractionation), the fractionation was zero. This was explained by a rate-dependent kinetic effect (Skulan et al., 2002). The disagreement between the theoretical equilibrium effects, predicting light Fe in hematite, and the experimental results, predicting light Fe only during a kinetic fractionation, might be explained by an inaccuracy in the Mössbauer-derived mineral fractionation factors, or in the experiments (Anbar et al., 2005). Bullen et al. (2001) have measured a bulk fractionation factor $\Delta_{Fe(III)OOH-Fe(II)aq}$ of +1‰ for the oxidation of $Fe(II)_{aq}$ to Fe(III)OOH in both laboratory experiments and a natural stream situation. This bulk fractionation is compatible with the combination of fractionation effects by (1) formation of a dissolved oxidation product, i.e., Fe(III) species in solution, enriched in ^{56}Fe, followed by (2) kinetically controlled precipitation of a solid Fe(III)OOH depleted in ^{56}Fe (Beard and Johnson, 2004). The equilibrium reduction of solid ferric iron cannot be simulated easily, and preliminary experiments have involved dissimilatory iron-reducing bacteria to induce the reduction. The relative direction of this reductive fractionation is opposite to that determined for iron oxidation, and is also similar in magnitude (Johnson et al., 2004b). These results are entirely consistent with the general observation of redox reactions producing the largest, and possibly reversible, iron isotope effects. A non-redox-related fractionation factor is that of $Fe(II)_{aq}$ adsorption onto a solid, for which an experimental $\Delta_{Fe(II)sorbed-Fe(II)aq}$ value of −2‰ was determined (Johnson et al., 2005). This, again, is interpreted to reflect a kinetic effect. A very different result was obtained for adsorption of Fe(II) onto goethite, which resulted in $\Delta_{Fe(II)sorbed-Fe(II)aq}$ of +1.5‰ to +2.5‰ (Icopini et al., 2004). The disagreement between these two estimates is still a matter of intense debate (Johnson et al., 2005). Finally, the precipitation of siderite from $Fe(II)_{aq}$ was predicted from spectroscopic data to result in siderite that is approximately 1.5‰ lighter than the iron dissolved in the fluid (Polyakov and Mineev, 2000; Schauble et al., 2001). A preliminary experimental determination of this isotope fractionation resulted in $\Delta_{siderite-Fe(II)aq}$ of −0.5‰ (Wiesli et al., 2004).

The fractionation upon weathering was simulated experimentally by exposing hornblende and goethite to a variety of leaching reagents (acetate, oxalate, citrate, and the siderophore desferrioxamine mesylate; Brantley et al., 2001; Brantley et al., 2004). Leaching of hornblende released fluids that were lighter by 0.1–1.2‰, while no fractionation occurred upon leaching of goethite (Brantley et al., 2004).

6.1.3. Solid–solid fractionation

These fractionation factors are entirely based on predictions from spectroscopic data (Polyakov, 1997). For the minerals measured in this study the following equilibrium fractionation factors are predicted at 25 °C presented relative to Fe(III)aq = 0‰ using the reduced partition function of Anbar et al. (2005): siderite = −4.9‰; goethite = −3.4‰; hematite = −1.9‰; pyrite = +1.8‰. At 250 °C, the sequence is siderite = −1.8‰; goethite = −1.3‰; hematite = −0.6‰; pyrite = +0.7‰.

6.2. Iron isotope fractionation pathways

We can now proceed to evaluate the measured data in view of these fractionation factors. We do this by first establishing possible iron isotopic compositions of the hydrothermal fluid. Then, we proceed to discuss how chemical reactions in the fluids are involved in the modification of these compositions.

6.2.1. Leaching of iron from the basement

Silicate rocks usually contain unfractionated iron ($\delta^{56}Fe_{IRMM14} = +0.09‰$; Beard et al., 2002). Recently, some heavily differentiated granites have been measured of which $\delta^{56}Fe$ ranges between +0.1‰ and +0.38‰ (Poitrasson and Freydier, 2005). This is the range we assume for the composition of leached basement rocks. The exper-

imental fractionation factors outlined above appear to indicate that leaching of silicates would produce fluids that are slightly depleted in ^{56}Fe over ^{54}Fe by 1‰ at the most, but that leaching of oxides would not entail an isotope fractionation. For the case of hydrothermal leaching of Fe from rock-forming basement minerals such as amphibole, biotite, Fe-oxides or pyroxenes appears to result in $Fe(II)_{aq}$ of slightly lighter compositions (Rouxel et al., 2003). Quantitative hydrothermal dissolution of silicates, however, would result in an iron-bearing fluid of unfractionated compositions. Overall, fluid–rock interaction involving a relatively reduced fluid would be expected to result in a Fe isotope composition of around 0‰ to −0.5‰ (maximum −1.0‰).

The thermodynamic modeling has shown that all leached Fe is in the ferrous state, and that the vast majority of leached fluids is within the $FeCl_2$ predominance field (Fig. 6). $FeCl_2$ would fractionate Fe by ca. −1‰ relative to the Fe(II)-hexaquo complex. However, if the transfer of iron from basement to fluid entails immediate and quantitative formation of the chloro complex, the fluids would preserve the isotopic composition of the leached iron without further modification. The high salinities of 20–40 wt% NaCl equivalent further ensure a high degree of mobility of these fluids (Yardley, 2005). We would, therefore, expect a high availability of iron having a relatively homogenous isotopic composition in the fluid. The large range of observed inter-mineral and within-mineral variations in the hydrothermal veins, however (Fig. 4), which are furthermore not in the sequence as suggested from inter-mineral fractionation factors, seem to suggest that these fluids are strongly modified by secondary processes. Minerals precipitated from these fluids trace these fluids' composition.

6.2.2. Fluid mixing with surface water

Partial oxidation of fluids by oxidized surface waters would form $Fe(III)_{aq}$ that should be around 3‰ heavier at 25 °C, or 1.5‰ heavier at 250 °C. The model for O_2-saturated fluids (left column in Fig. 7) show that hematite forms at this stage. Fractionation factors for hematite formation suggest slightly lighter compositions for hematite than the $Fe(III)_{aq}$. Therefore, an overall maximum fractionation of +1.5‰ would be expected for the solids precipitating from the Fe(II)-bearing solutions. Given that primary fluids are predicted to have compositions of −0.5‰ to 0‰, hematite precipitating at equilibrium is predicted to contain iron with $\delta^{56}Fe$ of ca. +0.5‰ to +1.0‰. In our samples, the range of measured $\delta^{56}Fe$ in primary hydrothermal hematite is larger with −0.5‰ to +0.5‰. These in part lighter compositions can be explained by mass balance effects. Only if the fraction of Fe(II) oxidized and precipitated is small, compositions that are close to the predicted fractionation factors would result. If the fraction of Fe oxidized and precipitated is large, the hematite formed will obtain a composition close to that of the fluid. Indeed it has been shown that a significant drop in Fe(II) occurs if the fraction of the oxidizing surface fluid (fluid2 on Fig. 7) is larger than 70%, and most of the Fe dissolved in the fluid would be transferred into hematite.

We illustrate the composition of a solid formed during a given mineralization event at various degrees of $Fe(II)_{aq}$ remaining in solution after oxidation in a Rayleigh-type calculation (Fig. 9). The grey curve gives an example for bulk hematite ($\Delta_{hematite-Fe(II)aq} = +1.5$) precipitating from an oxidized Fe(II) fluid with an initial $\delta^{56}Fe$ of −0.5‰. This resulting hematite has a composition of between +1 (the fraction of oxidized and precipitated $Fe(II)_{aq}$ is small) and −0.5‰ (all $Fe(II)_{aq}$ oxidized and precipitated). This is exactly the range observed for primary hematite. In this simple scenario, the Fe isotope compositions would serve as proxy for the degree of fluid oxidation and Fe precipitation. However, more complex scenarios are also possible in which the ferrous Fe fluid is oxidized in separate stages. Then, the later generations of hematite would precipitate from residual fluids depleted in heavy Fe during previous oxidation events. The bulk hematites formed would integrate over a series of compositional increments (indicated by the progressively evolving instantaneous precipitate). Based on this model, it is not surprising that an individual mineral from one sample may show highly variable iron isotopic compositions, even in the primary, high-temperature minerals. For example, primary, euhedral hematite from the Rappenloch deposit shows surprisingly variable iron isotopic compositions. In a single hand-sized layered ore specimen larger crystals in a vuggy layer have a $\delta^{56}Fe$ of +0.04‰, whereas a microcrystalline layer has a value of −0.11‰. Another typical coarse-grained primary hematite from the same location has a value of −0.28‰.

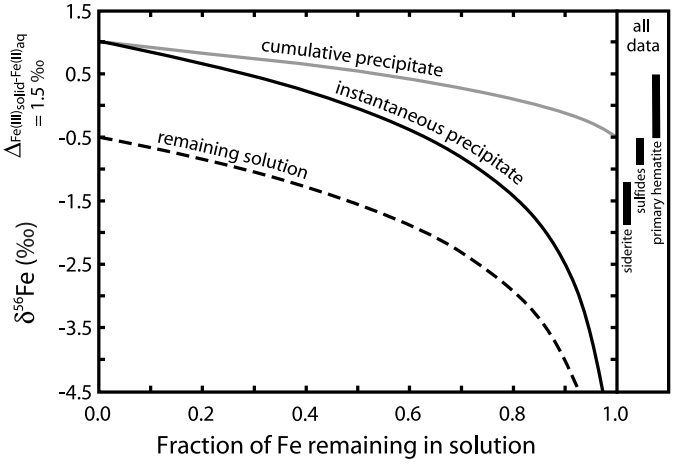

Fig. 9. Rayleigh-type calculation showing the composition of a solid formed at various degrees of Fe(II)aq remaining in solution after oxidation. The grey curve gives an example for bulk hematite ($\Delta_{hematite-Fe(II)aq} = +1.5$) precipitating from an oxidized Fe(II) fluid with an initial $\delta^{56}Fe$ of 0.5‰. This hematite obtains an integrated composition of between +1 (fraction $Fe(II)_{aq}$ oxidized and precipitated is small) and 0.5‰ (all $Fe(II)_{aq}$ oxidized and precipitated). The later generations of hematite would precipitate from residual fluids depleted in heavy Fe during previous oxidation events (instantaneous precipitate). The remaining fluid will always have the composition of the lower, dashed curve.

The setting for carbonate and sulfide precipitation is quite different. These do not involve an oxidation step. The right column in Fig. 7 shows that siderite precipitates from reduced surface fluids that have dissolved carbonate from overlying sediments and are enriched in HCO_3^- and CO_3^{2-}. Equilibrium fractionation factors suggest that siderite incorporates light iron relative to a Fe(II)-bearing fluid ($\Delta_{siderite-Fe(II)aq} = -4.9‰$ to $-0.5‰$). Indeed, measured siderite contains light iron throughout ($\delta^{56}Fe = -1.4‰$ to $-0.7‰$), but the heavy Fe of this range is not as light as would be expected if siderite precipitated from an initial fluid of $-0.5‰$ with a fractionation factor of $\leqslant 0.5‰$. One reason might be that the measured siderites formed from fluids that always transferred a substantial fraction of their $Fe(II)_{aq}$ into the siderite, thereby not resulting in any net isotope fractionation due to mass balance constraints. In any case, the composition of the siderites, namely, the absence of very light compositions that might potentially have formed by precipitating siderite from an oxidizing fluid that has experienced depletion in heavy Fe (the curve labelled remaining solution in Fig. 9) is entirely compatible with the inferred formation process. Unlike hematite formation that involves oxidizing surficial fluids (left column in Fig. 7), siderite precipitates from HCO_3^--enriched fluids. The siderite compositions confirm that the siderites precipitated from non-oxidizing environments, as predicted by the thermodynamic model.

It can be assumed that sulfides (chalcopyrite, pyrite) precipitated from reduced, sulfide-rich hydrothermal solutions. Chalcopyrite and pyrite both contain iron with $\delta^{56}Fe$ of $-0.3‰$ to $0‰$. Based on the fractionation factors discussed above it is expected that sulfides would incorporate iron that is much heavier than found in the Fe(II) fluid from which they precipitate and that is also heavier than hematite. Considering that this is not observed, these isotope compositions are compatible with near-quantitative precipitation from a fluid of light initial composition.

6.2.3. High-temperature alteration

Three hematite samples from Table 1 were interpreted to show a high-temperature alteration of primary Fe minerals. They cover a range in $\delta^{56}Fe$ between $+0.5‰$ and $+0.9‰$. The texturally most convincing evidence for high-temperature alteration is shown sample M590 from the Sophia mine near Wittichen. In this sample, very thin leaf-like hematite ($\delta^{56}Fe$: $+0.81‰$) is found as oxidation product on an earlier generation of siderite ($\delta^{56}Fe$: -1.36) and is also overgrown by a younger generation of siderite ($\delta^{56}Fe$: $-0.74‰$). Both siderites are interpreted as being of high-temperature origin (>150 °C). This is based on textural observations and on fluid inclusion studies. The older siderite generation shows dark brown patches resulting from partial oxidation and thus we suggest that the hematite formed via oxidation of the first generation siderite during a relatively oxidizing event of the high-temperature, vein-filling processes. The second generation of siderite was then precipitated during a new influx of reduced, CO_2-bearing fluid. The rather high $\delta^{56}Fe$ value of the hematite is confirmed by texturally identical hematite from the mineralogically similar Anton mine ($\delta^{56}Fe$: $+0.84‰$) which is situated close to the Sophia mine and by a texturally similar hematite from the Clara mine ($\delta^{56}Fe$: $+0.9‰$). The isotopic difference between siderite and high-temperature secondary hematite of $+1.6‰$ to $+2.3‰$ lies exactly in the range predicted from the above-mentioned siderite–hematite fractionation factors. This indicates that siderite and hematite achieved thermodynamic equilibrium during this fluid-assisted high-temperature alteration process. At thermodynamic equilibrium and exchange of Fe between both minerals involved, mineral isotope compositions would reflect the relative equilibrium fractionation factors of these minerals.

6.2.4. Low-temperature alteration

The situation is entirely different during low-temperature alteration, where no chemical equilibrium is established. The thermodynamic model (Fig. 8) has shown that goethite replaces siderite when exposed to oxidizing fluids, and that no Fe is released in the process. In that case we would expect that goethite exactly inherits the Fe isotope composition of the siderite precursor, despite the fractionation factor that would predict goethite that is $1.5‰$ heavier than siderite at 25 °C. This is exactly the pattern that is observed. Secondary goethite yields a range in $\delta^{56}Fe$ of $-1.1‰$ to $-0.5‰$, very similar to primary siderites that range from $-1.36‰$ to $-0.7‰$. Therefore, these goethite compositions demonstrate the feasibility of the suggested alteration processes. Furthermore, it appears that replacement products serve to identify the Fe isotope composition of their precursor (provided that no additional Fe is brought into the system by the oxidizing alteration fluid).

Within the Clara mine, alteration of primary sulfides ($\delta^{56}Fe$ around $-0.3‰$) led to precipitation of the secondary, supergene Fe(III)-arsenates Ba-pharmacosiderite and scorodite ($\delta^{56}Fe$: $-0.16‰$ and $-0.24‰$), partly on pseudomorphed chalcopyrite, partly some cm to dm away from it. Given that the isotope compositions of the alteration products are so similar to their precursors, we can assume that a complete iron transfer has taken place between the two. A detailed description of iron isotope systematics within single deposits can be found in Appendix A.

6.2.5. Sedimentary Fe deposits

Oolithic iron ores of the Dogger (Middle Jurassic) contain goethites which have $\delta^{56}Fe$ values between $+0.02‰$ and $+0.42‰$. This range is close to crystalline rocks ($\delta^{56}Fe$: $+0.04‰$ to $+0.38‰$; Beard et al., 2002; Poitrasson and Freydier, 2005), and also close to the range of modern clastic marine sediments ($\delta^{56}Fe$: $-0.2‰$ to $+0.3‰$; Beard and Johnson, 2004). We suggest the following evolution to explain these features: (1) dissolved iron is homogenized during transport, or is derived from isotopically uniform sources, resulting in relatively uniform pre-oxidation isotope ratios, (2) $Fe(II)_{aq}$ is oxidized, with $Fe(III)_{aq}$ being

about 3‰ heavier, and (3) goethite is precipitated from $Fe(III)_{aq}$, with $\delta^{56}Fe$ being about −3.4‰ lighter than $Fe(III)_{aq}$ at equilibrium. Steps (2) and (3) compensate each other isotopically (depending on the actual mass balances and potential further kinetic fractionation effects), such that goethite is deposited with $\delta^{56}Fe$ close to that of the original seawater. Another, equally speculative explanation is that the dissolved (e.g., coastal) $Fe(II)_{aq}$ was always immediately and quantitatively oxidized and precipitated into goethite, such that the original dissolved Fe compositions are now preserved by the goethite. Finally, it is possible that oolite formation involves diagenetic reactions, which might fractionate iron towards light compositions on reduction, and towards heavy compositions on re-oxidation and precipitation into oolitic Fe(III).

7. Summary and conclusion

Iron isotopes in hydrothermal mineralizations encompass a range of 2.5‰ in $\delta^{56}Fe$ values. Given that such variability occurs within single veins, sometimes even within an individual layered hematite sample, we can discount the possibility that these isotope ratios provide information on the iron source (Graham et al., 2004). Rather, we suggest a scenario in which the iron isotopes trace the fluid history. This first entails leaching of Fe from basement. The resulting fluids are rich in Cl to which $Fe(II)_{aq}$ is strongly bound ($\delta^{56}Fe = -0.5‰$). These hydrothermal fluids can precipitate Fe mineral through two different depositional mechanisms. One is mixing with oxygen-rich surface waters, resulting in the precipitation of isotopically heavy hematite. The second is input of CO_2-rich fluids (produced by surface carbonate sediment dissolution) which leads to the precipitation of light siderite. Given that the two precipitation products are isotopically distinct (heavy hematite and light siderite, respectively), their composition serves to trace the responsible depositional mechanisms. The residual fluids can be further oxidized, or they can be recharged by fresh iron-rich hydrothermal fluids of unfractionated composition. Therefore, a large range of mixing ratios can be produced. Such mixing histories are recorded at the meter scale by isotope differences between minerals of the same generation, on the cm scale by differences between minerals within one hand specimen, and on the millimeter scale by intimately zoned hematite and goethite aggregates. Magnetite is never formed as this would require either low f_{O_2} (carbonate-free fluids) or high f_{O_2} (carbonate-bearing fluids).

Secondary alteration products are goethite and hematite, which form by replacement of siderite at both high and low temperatures. The low-T secondary minerals appear to inherit the composition of their precursors throughout. Therefore, Fe isotopes can serve to identify precursors in such replacement reactions. In contrast, high-T alteration produces replacement products at thermodynamic equilibrium. The Fe isotope composition of these products (hematite, goethite) is different from that of the precursor (siderite) by the predicted fractionation factor.

Finally, the range of compositions of goethite from oolitic iron ores seems to indicate oxidative precipitation from a relatively uniform coastal water Fe reservoir. Unlike Fe isotopes that equilibrate under metamorphic or magmatic conditions, the iron isotope systematics found when hydrothermal fluids are involved shows remarkable variations. Importantly, these variations are consistent with both thermodynamic formation models and predicted Fe isotope fractionation factors. Therefore, Fe isotopes have considerable potential as tracers of ore-forming processes.

Acknowledgments

We are grateful to Marc Mamberti and Ronny Schoenberg for their support of the Fe isotope analyses presented here. We acknowledge the constructive reviews by S. Kesler, B. Bergquist, C. Smith, O. Rouxel, and an anonymous reviewer.

Associate editor: Martin B. Goldhaber

Appendix A. Detailed description of iron isotope systematics in single deposits

In the following section, we describe iron isotopic variations within single deposits. Samples from the Clara mine show the largest variability of all deposits investigated. Weathering of primary sulfides ($\delta^{56}Fe$ around −0.3‰) led to precipitation of secondary, supergene Fe(III)-arsenates Ba-pharmacosiderite and scorodite ($\delta^{56}Fe$: −0.16‰ and −0.24‰) partly on pseudomorphed chalcopyrite, partly some cm to dm away from it. Alteration and oxidation of primary siderite in the Clara mine ($\delta^{56}Fe = -0.99‰$) results in significant shifts of the Fe isotopic composition. Siderite, which is dark brown and hence partially oxidized to goethite, exhibits a $\delta^{56}Fe$ of −0.8‰, which is also the value of secondary goethite. Secondary fibrous hematite has an even heavier value of −0.66‰.

Four samples from the Sophia mine near Wittichen comprise three siderites and one hematite. Of those, two siderites and the hematite come from the same hand specimen (M590). The hematite ($\delta^{56}Fe = +0.81‰$) is found as oxidation product on an earlier generation of siderite ($\delta^{56}Fe = -1.36$) directly overgrown by a younger generation of siderite ($\delta^{56}Fe = -0.74‰$). The very heavy value of the hematite is confirmed by texturally identical hematite from the Anton mine ($\delta^{56}Fe = +0.84‰$) which is situated close to the Sophia mine. Both mined almost identical Co–Ag-barite veins. A partly oxidized siderite from a different sample in the Sophia mine is slightly isotopically lighter ($\delta^{56}Fe = -0.85‰$), which, however, might also be a primary feature not related to the oxidation. The siderite–hematite combination implies that there is a very significant isotopic fractionation during common precipitation

of minerals containing iron in different valence states which qualitatively agrees with the results from the Clara mine detailed above.

At the barite–goethite deposit of Neuenbürg, partially oxidized siderite (−0.83‰ to −0.72‰), secondary fibrous crystalline hematite (−0.24‰ and −0.44‰) and secondary fibrous goethite (−0.64‰) have values in the same range, but hematite is heavier than the siderite as was also observed in the Clara and Sophia mine samples. This shows that the oxidation processes operate in a similar way in very different types of deposits. Obviously, mass balance dependent equilibrium fractionation leads to successively heavier Fe isotopic compositions during oxidation of the primary iron-bearing minerals.

On the other hand, two localities appear to tell a different story. At the Otto mine, large euhedral, primary hematite crystals have a δ^{56}Fe value of +0.3‰, whereas microcrystalline, most probably secondary hematite from the same sample has a δ^{56}Fe of −0.97‰. Fibrous secondary goethite from another sample has a value of −1.12‰.

Similarly, the Kienberg sample FE8 shows large variations in the same direction towards lighter values within millimeters; older fibrous goethite (δ^{56}Fe = −0.52‰) is overgrown by feathery hematite (δ^{56}Fe = −1.08‰).

Primary, euhedral hematite from the Rappenloch mine shows surprisingly variable iron isotopic compositions. In a single hand-sized layered ore specimen larger crystals in a vuggy layer have a δ^{56}Fe of +0.04‰, whereas a microcrystalline layer has a value of −0.11‰. Another typical coarse-grained primary hematite from the same location has a value of −0.28‰. A sample of layered, fibrous hematite of secondary origin from the Rappenloch mine has a value of −0.78‰, whereas all primary hematites vary only between −0.28‰ and +0.04‰. Centimeter-sized crystals of a different sample from Farrenberg near Eisenbach (same mineralization type as Rappenloch, 500 m apart from each other) have a δ^{56}Fe value of +0.01‰, i.e., identical to the crystalline layer in the aforementioned sample. Two further samples of layered, botroidal hematite (''red glaskopf'') have δ^{56}Fe values of −0.28‰ and −0.78‰, respectively. Hence, one mineral not only from the same mining district, but also from the same mine and even from the same sample show highly variable iron isotopic compositions.

References

Albarède, F., 2004. The stable isotope geochemistry of Copper and Zinc. In: Johnson, C.M., Beard, B.L., Albarède, F. (Eds.), *Geochemistry of Non-Traditional Stable Isotopes*, vol. 55. Mineralogical Society of America, Washington, DC, pp. 409–427.

Anbar, A.D., 2004. Iron stable isotopes: beyond biosignatures. *Earth Planet. Sci. Lett.* **217**, 223–226.

Anbar, A.D., Jarzecki, A.A., Spiro, T.G., 2005. Theoretical investigation of iron isotope fractionation between $Fe(H_2O)^{3+}6$ and $Fe(H_2O)^{2+}6$: implications for iron stable isotope geochemistry. *Gechim. Cosmochim. Acta* **69**, 825–837.

Barling, J., Arnold, G.L., Anbar, A.D., 2001. Natural mass-dependent variations in the isotopic composition of molybdenum. *Earth Planet. Sci. Lett.* **193**, 447–457.

Beard, B.L., Johnson, C.M., 2004. Fe isotope variations in modern and ancient Earth and other planetary bodies. In: Johnson, C.M., Beard, B.L., Albarède, F. (Eds.), *Geochemistry of Non-Traditional Stable Isotopes*, vol. 55. Mineralogical Society of America, Washington, DC, pp. 319–357.

Beard, B.L., Johnson, C.M., Skulan, J.L., Nealson, K.H., Cox, L., Sun, H., 2002. Application of Fe isotopes to tracing the geochemical and biological cycling of Fe. *Chem. Geol.* **195**, 87–117.

Bliedtner, M., Martin, M., 1988. *Erz—und Minerallagerstätten des Mittleren Schwarzwaldes*. Geologisches Landesamt Baden-Wuerttemberg, Freiburg i.Br.

Brantley, S.L., Liermann, L.J., Bullen, T.D., 2001. Fractionation of Fe isotopes by soil microbes and organic acids. *Geology* **29**, 535–538.

Brantley, S.L., Liermann, L.J., Guynn, R.L., Anbar, A.D., Icopini, G.A., Barling, J., 2004. Fe isotope fractionation during mineral dissolution with and without bacteria. *Geochim. Cosmochim. Acta* **68**, 3189–3204.

Bullen, T.D., White, A.F., Childs, C.W., Vivit, D.V., Schulz, M.S., 2001. Demonstration of significant abiotic iron isotope fractionation in nature. *Geology* **29**, 699–702.

Ellis, A.S., Johnson, T.M., Bullen, T.D., 2002. Chromium isotopes and the fate of hexavalent chromium in the environment. *Science* **295** (5562), 2060–2062.

Emmermann, R., 1977. A petrogenetic model for the origin and evolution of the Hercynian granite series of the Schwarzwald. *N. Jahrb. Mineral. Abh.* **128**, 219–253.

Graham, S., Pearson, N., Jackson, S., Griffin, W., O'Reilly, S., 2004. Tracing Cu and Fe from source to porphyry: in situ determination of Cu and Fe isotope ratios in sulfides from the Grasberg Cu–Au deposit. *Chem. Geol.* **207**, 147–169.

Hoefs, J., Emmermann, R., 1983. The oxygen isotope composition of Hercynian granites and pre-Hercynian gneisses from the Schwarzwald, SW Germany. *Contrib. Mineral. Petrol.* **83**, 320–329.

Hofmann, B., Eikenberg, J., 1991. The Krunkelbach uranium deposit, Schwarzwald, Germany. Correlation of radiometric ages, U–Pb, U–Xe–Kr, K–Ar, Th–U with mineralogical stages and fluid inclusions. *Econ. Geol.* **86**, 1031–1049.

Holland, T.J.B., Powell, R., 1998. An internally consistent thermodynamic data set for phases of petrological interest. *J. Metam. Geol.* **16**, 309–343.

Icopini, G.A., Anbar, A.D., Ruebush, S.S., Tien, M., Brantley, S.L., 2004. Iron isotope fractionation during microbial reduction of iron: the importance of adsorption. *Geology* **32**, 205–208.

Johnson, C.M., Beard, B.L., Albarède, F., 2004a. Geochemistry of non-traditional stable isotopes. In: Rosso, J.J. (Ed.), *Reviews in Mineralogy and Geochemistry*, vol. 55. Mineralogical Society of America, Washington, DC.

Johnson, C.M., Beard, B.L., Roden, E.E., Newman, D.K., Nealson, K.H., 2004b. Isotopic constraints on biogeochemical cycling of Fe. In: Johnson, C.M., Beard, B.L., Albarède, F. (Eds.), *Geochemistry of Non-Traditional Stable Isotopes*, vol. 55. Mineralogical Society of America, Washington, DC, pp. 359–408.

Johnson, C.M., Beard, B.L., Welch, S.A., Roden, E.E., Croal, L.R., Newman, D.K., Nealson, K.H., 2005. Experimental constraints on Fe isotope fractionation during magnetite and Fe carbonate formation coupled to dissimilatory hydrous ferric oxide reduction. *Geochim. Cosmochim. Acta* **69**, 963–993.

Johnson, J.W., Oelkers, E.H., Helgeson, H.C., 1992. SUPCRT92: A software package for calculating the standard molal thermodynamic properties of minerals, gases, aqueous species, and reactions from 1 to 5000 bar and 0 to 1000 °C. *Comp. Geosci.* **18**, 899–947.

Lippolt, H.J., Kirsch, H., 1994. Isotopic Investigation of Post-Variscan Plagioclase Sericitization in the Schwarzwald Gneiss Massif. *Chem. Erde* **54**, 179–198.

Maréchal, C.N., Nicolas, E., Douchet, C., Albarède, F., 2000. Abundance of zinc isotopes as a marine biogeochemical tracer. *Geochem. Geophys. Geosyst.* **1**, 1999GC000029.

Markl, G., 2004. Wie kommt das Silber ins Gestein? Die Bildung der Schwarzwälder Erzgänge und ihrer Mineralien. In: Markl, G., Lorenz,

S. (Eds.), *Silber Kupfer Kobalt—Bergbau im Schwarzwald*. Markstein Verlag, Filderstadt.

Matthews, A., Zhu, X.K., O'Nions, R.K., 2001. Kinetic iron stable isotope fractionation between iron (-II) and (-III) complexes in solution. *Earth Planet. Sci. Lett.* **192**, 81–92.

Meshik, A.P., Lippolt, H.J., Dymkov, Y.M., 2000. Xenon geochronology of Schwarzwald pitchblendes. *Mineral. Deposita* **35**, 190–205.

Metz, R., Richter, M., Schürenberg, H., 1957. Die Blei- Zink- Erzgänge des Schwarzwaldes. *Beih. Geol. Jahrb.* **29**, 1–277.

Meyer, M., Brockamp, O., Clauer, N., Renk, A., Zuther, M., 2000. Further evidence for a Jurassic mineralizing event in central Europe. K–Ar dating of geothermal alteration and fluid inclusion systematics in wall rocks of the Käferteige fluorite vein deposit in the northern Black Forest, Germany. *Mineral. Deposita* **35**, 754–761.

Oelkers, E.H., Helgeson, H.C., 1990. Triple-ion anions and polynuclear complexing in supercritical electrolyte solutions. *Geochim. Cosmochim. Acta* **54**, 727–738.

Poitrasson, F., Freydier, R., 2005. Heavy iron isotope composition of granites determined by high resolution MC-ICP-MS. *Chem. Geol.* **222**, 132–147.

Polyakov, V.B., 1997. Equilibrium fractionation of the iron isotopes: estimation from Mössbauer spectroscopy data. *Geochim. Cosmochim. Acta* **61**, 4213–4217.

Polyakov, V.B., Mineev, S.D., 2000. The use of Mössbauer spectroscopy in stable isotope geochemistry. *Geochim. Cosmochim. Acta* **64**, 849–865.

Rouxel, O., Dobbek, N., Ludden, J., Fouquet, Y., 2003. Iron isotope fractionation during oceanic crust alteration. *Chem. Geol.* **202**, 155–182.

Schauble, E.A., 2004. Applying stable isotope fractionation theory to new systems. In: Johnson, C.M., Beard, B.L., Albarède, F. (Eds.), *Geochemistry of Non-Traditional Stable Isotopes*, vol. 55. Mineralogical Society of America, Washington, DC, pp. 65–111.

Schauble, E.A., Rossmann, G.R., Taylor, H.P., 2001. Theoretical estimates of equilibrium Fe-isotope fractionations from vibrational spectroscopy. *Geochim. Cosmochim. Acta* **65**, 2487–2497.

Schoenberg, R., von Blanckenburg, F., 2005. An assessment of the accuracy of stable Fe isotope ratio measurements on samples with organic and inorganic matrices by high-resolution multicollector ICP-MS. *Intern. J. Mass Spectrom.* **242**, 257–272.

Schwinn, G., Markl, G., 2005. REE systematics in hydrothermal fluorite. *Chem. Geol.* **216**, 225–248.

Schwinn, G., Wagner, T., Baldorj, B., Markl, G., 2006. Quantification of mixing processes in ore-forming hydrothermal systems by combination of stable isotope and fluid inclusion analyses. *Geochim. Cosmochim. Acta* **70**, 965–982.

Segev, A., Halicz, L., Lang, B., Steinitz, G., 1991. K–Ar dating of manganese minerals from the Eisenbach region, Black Forest, southwest Germany. *Schweiz. Mineral. Petrogr. Mitt.* **71**, 101–114.

Seward, T.M., Barnes, H.L., 1997. Metal transport in hydrothermal ore fluids. In: Barnes, H.L. (Ed.), *Geochemistry of Hydrothermal Ore Deposits*, third ed. Wiley, New York, pp. 435–486.

Shock, E.L., Oelkers, E.H., Johnson, J.W., Sverjensky, D.A., Helgeson, H.C., 1992. Calculation of the thermodynamic properties of aqueous species at high pressures and temperatures. *J. Chem. Soc. Faraday Transact.* **88**, 803–826.

Shock, E.L., Sassani, D.C., Willis, M., Sverjensky, D.A., 1997. Inorganic species in geological fluids: correlations among standard molal thermodynamic properties of aqueous ions and hydroxide complexes. *Geochim. Cosmochim. Acta* **61**, 907–950.

Shvarov, Y.V., 1978. Minimization of the thermodynamic potential of an open chemical system. *Geochem. Internat.* **15**, 200–203.

Shvarov, Y.V., 1981. A general equilibrium criterion for an isobaric-isothermal model of a chemical system. *Geochem. Internat.* **18**, 38–45.

Shvarov, Y., Bastrakov, E., 1999. HCh: a software package for geochemical equilibrium modeling. User's guide. Australian Geological Survey Organisation, Record 1999/25, 61 p.

Simon, K., Hoefs, J., 1987. Effects of meteoric water interaction on Hercinian granites from the Südschwarzwald, Southwest Germany. *Chem. Geol.* **61**, 253–261.

Skulan, J.L., Beard, B.L., Johnson, C.J., 2002. Kinetic and equilibrium Fe isotope fractionation between aqueous Fe(III) and hematite. *Geochim. Cosmochim. Acta* **66**, 2995–3015.

Sverjensky, D.A., Shock, E.L., Helgeson, H.C., 1997. Prediction of the thermodynamic properties of aqueous metal complexes to 1000 °C and 5 kb. *Geochim. Cosmochim. Acta* **61**, 1359–1412.

Tagirov, B., Schott, J., 2001. Aluminum speciation in crustal fluids revisited. *Geochim. Cosmochim. Acta* **65**, 3965–3992.

Wagner, T., Boyce, A.J., 2003. Sulphur isotope geochemistry of black shale-hosted antimony mineralization, Arnsberg, northern Rhenish Massif, Germany: implications for late-stage fluid flow during the Variscan orogeny. *J. Geol. Soc. London* **160**, 299–308.

Wagner, T., Cook, N.J., 2000. Late-Variscan antimony mineralization in the Rheinisches Schiefergebirge, NW Germany: Evidence for stibnite precipitation by drastic cooling of high-temperature fluid systems. *Mineral. Deposita* **35**, 206–222.

Walczyk, T., von Blanckenburg, F., 2002. Natural iron isotope variations in human blood. *Science* **295**, 2065–2066.

Walczyk, T., von Blanckenburg, F., 2005. Deciphering the iron isotope message of the human body. *Intern. J. Mass Spectrom.* **242**, 117–134.

Welch, S.A., Beard, B.L., Johnson, C.M., Braterman, P.S., 2003. Kinetic and equilibrium Fe isotope fractionation between aqueous Fe(II) and Fe(III). *Geochim. Cosmochim. Acta* **67**, 4231–4250.

Werner, W., Dennert, V., 2004. *Lagerstätten und Bergbau im Schwarzwald*. Landesamt für Geologie, Rohstoffe und Bergbau Baden-Württemberg, Freiburg, Germany, 334 p.

Werner, W., Franzke, H.J., 2001. Postvariskische bis neogene Bruchtektonik und Mineralisation im südlichen Schwarzwald. *Z. Dt. Geol. Ges.* **152**, 405–437.

Werner, W., Franzke, H.J., Wirsing, G., Jochum, J., Lüders, V., Wittenbrink, J., 2002. *Die Erzlagerstätte Schauinsland bei Freiburg im Breisgau*. Aedificatio Verlag, Freiburg.

Wernicke, R.S., Lippolt, H.J., 1993. Botryoidal hematite from the Schwarzwald, Germany. Heterogenous U distributions and their bearing on the helium dating method. *Earth Planet. Sci. Lett.* **114**, 287–300.

Wernicke, R.S., Lippolt, H.J., 1997. UTh-He evidence of a Jurassic continuous hydrothermal activity in the Schwarzwald basement, Germany. *Chem. Geol.* **138**, 273–285.

Wiesli, R.A., Beard, B.L., Johnson, C.M., 2004. Experimental determination of Fe isotope fractionation between aqueous Fe(II), siderite and "green rust" in abiotic systems. *Chem. Geol.* **211**, 343–362.

Williams, H.M., McCammon, C.A., Peslier, A.H., Halliday, A.N., Teutsch, N., Levasseur, S., Burg, J.P., 2004. Iron isotope fractionation and the oxygen fugacity of the mantle. *Science* **204**, 1656–1659.

Wood, S.A., Samson, I.M., 1998. Solubility of ore minerals and complexation of ore minerals in hydrothermal solutions. *Rev. Econ. Geol.* **10**, 33–80.

Yardley, B., 2005. Metal concentrations in crustal fluids and their relationship to ore formation. *Econ. Geol.* **100**, 613–632.

Zhu, X., Guo, Y., Williams, R., O'Nions, K., Matthews, A., Belshaw, N., Canters, G., de Waal, E., Weser, U., Burgess, B., Salvato, B., 2002. Mass fractionation processes of transition metal isotopes. *Earth Planet. Sci. Lett.* **200**, 47–62.

Zhu, X., O'Nions, K., Guo, Y., Belshaw, N., Rickard, D., 2000. Determination of natural Cu-isotope variation by plasma-source mass spectrometry: implications for use as geochemical tracers. *Chem. Geol.* **163**, 139–149.

Zuther, M., Brockamp, O., 1988. The fossil geothermal system of the Baden–Baden trough, northern Black Forest, Germany. *Chem. Geol.* **71**, 337–353.